Available online at www.sciencedirect.com
ScienceDirect
Journal of Computational Physics 225 (2007) 1863–1893
JOURNAL OF COMPUTATIONAL PHYSICS
www.elsevier.com/locate/jcp

Efficient and accurate numerical methods for the Klein–Gordon–Schrödinger equations

Weizhu Bao *, Li Yang

Department of Mathematics and Center for Computational Science and Engineering, National University of Singapore, Singapore 117543, Singapore

Received 26 November 2006; received in revised form 7 February 2007; accepted 21 February 2007
Available online 1 March 2007

Abstract

In this paper, we present efficient, unconditionally stable and accurate numerical methods for approximations of the Klein–Gordon–Schrödinger (KGS) equations with/without damping terms. The key features of our methods are based on: (i) the application of a time-splitting spectral discretization for a Schrödinger-type equation in KGS, (ii) the utilization of Fourier pseudospectral discretization for spatial derivatives in the Klein–Gordon equation in KGS, (iii) the adoption of solving the ordinary differential equations (ODEs) in phase space analytically under appropriate chosen transmission conditions between different time intervals or applying Crank–Nicolson/leap-frog for linear/nonlinear terms for time derivatives. The numerical methods are either explicit or implicit but can be solved explicitly, unconditionally stable, and of spectral accuracy in space and second-order accuracy in time. Moreover, they are time reversible and time transverse invariant when there is no damping terms in KGS, conserve (or keep the same decay rate of) the wave energy as that in KGS without (or with a linear) damping term, keep the same dynamics of the mean value of the meson field, and give exact results for the plane-wave solution. Extensive numerical tests are presented to confirm the above properties of our numerical methods for KGS. Finally, the methods are applied to study solitary-wave collisions in one dimension (1D), as well as dynamics of a 2D problem in KGS.

Keywords: Klein–Gordon–Schrödinger equations; Nonlinear Schrödinger equation; Klein–Gordon equation; Wave energy; Time splitting; Plane wave; Solitary wave; Unconditionally stable; Schrödinger–Yukawa equations

1. Introduction

The specific problem we study numerically is the Klein–Gordon–Schrödinger (KGS) equations describing a system of conserved scalar nucleons interacting with neutral scalar mesons coupled through the Yukawa interaction [31,15]:

* Corresponding author. Fax: +65 67746756.
E-mail addresses: bao@math.nus.edu.sg (W. Bao), yangli@nus.edu.sg (L. Yang).
URL: http://www.math.nus.edu.sg/~bao/ (W. Bao).

0021-9991/$ - see front matter © 2007 Elsevier Inc. All rights reserved.
doi:10.1016/j.jcp.2007.02.018

$$i\partial_t\psi + \Delta\psi + \phi\psi + iv\psi = 0, \quad \mathbf{x} \in \mathbb{R}^d, \ t > 0, \tag{1.1}$$

$$\varepsilon^2\partial_{tt}\phi + \gamma\varepsilon\partial_t\phi - \Delta\phi + \phi - |\psi|^2 = 0, \quad \mathbf{x} \in \mathbb{R}^d, \ t > 0, \tag{1.2}$$

$$\psi(\mathbf{x},0) = \psi^{(0)}(\mathbf{x}), \quad \phi(\mathbf{x},0) = \phi^{(0)}(\mathbf{x}), \quad \partial_t\phi(\mathbf{x},0) = \phi^{(1)}(\mathbf{x}), \ \mathbf{x} \in \mathbb{R}^d, \tag{1.3}$$

where the complex-valued unknown function $\psi = \psi(\mathbf{x},t)$ represents a scalar nucleon field, the real-valued unknown function $\phi = \phi(\mathbf{x},t)$ represents a scalar meson field, $\varepsilon > 0$ is a parameter inversely proportional to the speed of light, and γ and v are two nonnegative parameters. In fact, when $\varepsilon = 1, \gamma = 0$ and $v = 0$, it reduces to the standard KGS [15]. When $v > 0$, a linear damping term is added to the nonlinear Schrödinger equation (1.1) for arresting blowup. When $\gamma > 0$, a damping mechanism is added to the Klein–Gordon equation (1.2).

There was a series of mathematical study from partial differential equations for the KGS (1.1), (1.2) in the last two decades. For the standard KGS, i.e. $\varepsilon = 1, \gamma = 0$ and $v = 0$, Fukuda and Tsutsumi [14–16] established the existence and uniqueness of global smooth solutions, Biler [9] studied attractors of the system, Guo [17] established global solutions, Hayashi and Von Wahl [21] proved the existence of global strong solution, Guo and Miao [18] studied asymptotic behavior of the solution, Ohta [33] studied the stability of stationary states for KGS. For plane, solitary and periodic wave solutions of the standard KGS, we refer to [12,22,28,39]. For dissipative KGS, i.e. $\varepsilon = 1$, $\gamma > 0$ and $v > 0$, Guo and Li [19,27], Ozawa and Tsutsumi [34] studied attractor of the system and asymptotic smoothing effect of the solution, Lu and Wang [30] found global attractors. For the 'nonrelativistic' limit of the Klein–Gordon equation, we refer to [7,8,37,11].

In order to study effectively dynamics and wave interaction of the KGS, especially in 2D and 3D, an efficient and accurate numerical method is one of the key issues. However, numerical methods and simulation for the KGS in the literature remain very limited. Xiang [40] proposed a conservative spectral method for discretizating the standard KGS and established error estimate for the method. Zhang [41] studied a conservative finite difference method for the standard KGS in one dimension (1D). Due to that both methods are implicit, it is a little complicated to apply the methods for simulating wave interactions in KGS, especially in 2D and 3D. Usually, very tedious iterative method must be adopted at every time step for solving nonlinear system in the above discretizations for KGS and thus they are not very efficient. In fact, there was no numerical result for KGS based on their numerical methods in [40,41]. To our knowledge, numerical simulation results for KGS are very limited in the literature [25,10], especially in 2D and 3D as well as in the 'nonrelativistic' limit regime, i.e. $0 < \varepsilon \ll 1$. Thus, it is of great interests to develop an efficient, accurate and unconditionally stable numerical method for KGS. Such a numerical method is proposed here and it is applied to study the dynamics and wave interaction of the KGS (1.1)–(1.3). The key points in designing our new numerical methods are based on: (i) discretizing spatial derivatives in the Klein–Gordon equation (1.2) by Fourier pseudospectral method, and then solving the ordinary differential equations (ODEs) in phase space analytically under appropriate chosen transmission conditions between different time intervals or applying Crank–Nicolson/leap-frog for linear/nonlinear terms for time derivatives [5,4]; and (ii) solving the nonlinear Schrödinger equation (1.1) in KGS by a time-splitting spectral method [36,13,3,1], which was demonstrated to be very efficient and accurate and applied to simulate dynamics of Bose–Einstein condensation in 2D and 3D [2] and three-wave interactions in nonlinear optics [6,29]. Our extensive numerical results demonstrate that the methods are very efficient and accurate for KGS. In fact, similar techniques were already used for discretizing the Zakharov system [5,24] and the Maxwell–Dirac system [4,23].

The paper is organized as follows. In Section 2, we review some properties of the KGS equations and study dynamics of the mean value of the meson field. In Section 3, we present new efficient and accurate numerical methods for discretizing KGS. In Section 4, we study properties of our numerical discretization for KGS. In Section 5, we test the accuracy and stability of our methods for KGS with a solitary-wave solution, and apply them to study numerically dynamics of a plane wave, soliton–soliton collisions in 1D with/without damping terms and a 2D problem of KGS. Finally, some conclusions are drawn in Section 6.

2. Properties of the KGS equations

In this section, we will review some properties of the KGS equations (1.1)–(1.3) including time reversible, time transverse invariant, conservation laws, and plane and solitary waves in 1D. We also study dynamics of the mean value of the meson field and the 'nonrelativistic' limit of KGS.

(a) *Time reversible and time transverse invariant*. When $\gamma = 0$ and $v = 0$ in (1.1)–(1.3), the KGS is time reversible and time transverse invariant. If constants α and β are added to the initial data $\phi^{(0)}$ and $\phi^{(1)}$ in (1.3), respectively, i.e., $\phi^{(0)}(\mathbf{x}) \to \phi^{(0)}(\mathbf{x}) + \alpha$ and $\phi^{(1)}(\mathbf{x}) \to \phi^{(1)}(\mathbf{x}) + \beta$, then the solutions $\phi(\mathbf{x}, t)$ and $\psi(\mathbf{x}, t)$ obtained from (1.1)–(1.3) get added by $\alpha\cos(t/\varepsilon) + \beta\varepsilon\sin(t/\varepsilon)$ and multiplied by $e^{i\varepsilon(\alpha\sin(t/\varepsilon)-\beta\varepsilon\cos(t/\varepsilon))}$ respectively, i.e. $\phi(\mathbf{x}, t) \to \phi(\mathbf{x}, t) + \alpha\cos(t/\varepsilon) + \beta\varepsilon\sin(t/\varepsilon)$ and $\psi(\mathbf{x}, t) \to \psi(\mathbf{x}, t)e^{i\varepsilon(\alpha\sin(t/\varepsilon)-\beta\varepsilon\cos(t/\varepsilon))}$, which leaves the density $|\psi(\mathbf{x}, t)|^2$ unchanged.

(b) *Conservation laws*. When $\gamma = 0$ and $v = 0$ in (1.1)–(1.3), the KGS has at least two invariants which are the *wave energy*

$$D(t) := D(\psi(\cdot, t)) = \int_{\mathbb{R}^d} |\psi(\mathbf{x}, t)|^2 d\mathbf{x} \equiv \int_{\mathbb{R}^d} |\psi^{(0)}(\mathbf{x})|^2 d\mathbf{x} := D(0), \quad t \geqslant 0, \tag{2.1}$$

and the Hamiltonian

$$\begin{aligned} H(t) &= \int_{\mathbb{R}^d} \left[\frac{1}{2}(\phi^2(\mathbf{x}, t) + \varepsilon^2(\partial_t\phi(\mathbf{x}, t))^2 + |\nabla\phi(\mathbf{x}, t)|^2) + |\nabla\psi(\mathbf{x}, t)|^2 - |\psi(\mathbf{x}, t)|^2\phi(\mathbf{x}, t)\right] d\mathbf{x}, \\ &\equiv \int_{\mathbb{R}^d} \left[\frac{1}{2}((\phi^{(0)}(\mathbf{x}))^2 + \varepsilon^2(\phi^{(1)}(\mathbf{x}))^2 + |\nabla\phi^{(0)}(\mathbf{x})|^2) + |\nabla\psi^{(0)}(\mathbf{x})|^2 - |\psi^{(0)}(\mathbf{x})|^2\phi^{(0)}(\mathbf{x})\right] d\mathbf{x}, \\ &:= H(0), \quad t \geqslant 0. \end{aligned} \tag{2.2}$$

Furthermore, when $v > 0$, we have

$$D(t) := \int_{\mathbb{R}^d} |\psi(\mathbf{x}, t)|^2 d\mathbf{x} = e^{-2vt} \int_{\mathbb{R}^d} |\psi^{(0)}(\mathbf{x})|^2 d\mathbf{x} := e^{-2vt} D(0), \quad t \geqslant 0, \tag{2.3}$$

which implies $D(t)$ decay to 0 exponentially when $v > 0$. And when $\gamma > 0$ and $v = 0$, we have

$$H'(t) = \frac{dH(t)}{dt} = -\gamma\varepsilon \int_{\mathbb{R}^d} |\partial_t\phi(\mathbf{x}, t)|^2 d\mathbf{x} \leqslant 0, \quad t \geqslant 0, \tag{2.4}$$

which implies that $H(t)$ decreases when time t increases.

(c) *Plane-wave solution in 1D*. When $d = 1$, $\gamma = 0$, $v = 0$ and $\varepsilon = 1$ in (1.1)–(1.3), and the initial data in (1.3) is chosen as

$$\phi^{(0)}(x) = d > 0, \quad \phi^{(1)}(x) = 0, \quad \psi^{(0)}(x) = \sqrt{d}\exp\left(i\frac{2\pi lx}{b-a}\right), \quad x \in \mathbb{R}, \tag{2.5}$$

with l an integer, and a, b and d constants, the KGS admits the plane-wave solution [12]:

$$\phi(x, t) = d, \quad \psi(x, t) = \sqrt{d}\exp\left[i\left(\frac{2\pi lx}{b-a} - \omega t\right)\right], \quad x \in \mathbb{R}, \quad t \geqslant 0, \tag{2.6}$$

where

$$\omega = \left(\frac{2\pi l}{b-a}\right)^2 - d.$$

(d) *Solitary-wave solution in 1D*. When $d = 1$, $\gamma = 0$ and $v = 0$ in (1.1)–(1.3), the KGS admits the solitary-wave solution [22]

$$\psi_\pm(x, t) = 3B\,\mathrm{sech}^2(Bx + c_\pm t)\exp[i(d_\pm x + (4B^2 - d_\pm^2)t)], \tag{2.7}$$

$$\phi_\pm(x, t) = 6B^2\,\mathrm{sech}^2(Bx + c_\pm t), \quad x \in \mathbb{R}, \quad t \geqslant 0, \tag{2.8}$$

where

$$c_\pm = \pm\frac{\sqrt{4B^2-1}}{2\varepsilon} = \mathrm{O}\left(\frac{1}{\varepsilon}\right), \quad d_\pm = \mp\frac{\sqrt{4B^2-1}}{4B\varepsilon} = -\frac{c_\pm}{2B} = \mathrm{O}\left(\frac{1}{\varepsilon}\right),$$

with $B \geqslant 1/2$ a constant.

(e) *Dynamics of the mean value of the meson field when $v = 0$.* Define the mean value of the meson field as

$$N(t) := N(\phi(\cdot,t)) = \int_{\mathbb{R}^d} \phi(\mathbf{x},t)\mathrm{d}\mathbf{x}, \quad t \geqslant 0. \tag{2.9}$$

Integrating (1.2) over $\mathbb{R}^d$, integration by parts and noticing (2.3), we obtain

$$\varepsilon^2 N''(t) + \gamma\varepsilon N'(t) + N(t) = D(0), \quad t \geqslant 0, \tag{2.10}$$

with initial condition as

$$N(0) = N(\phi^{(0)}) := \int_{\mathbb{R}^d} \phi^{(0)}(\mathbf{x})\mathrm{d}\mathbf{x}, \quad N'(0) = N(\phi^{(1)}) := \int_{\mathbb{R}^d} \phi^{(1)}(\mathbf{x})\mathrm{d}\mathbf{x}. \tag{2.11}$$

Denote

$$\lambda_1^0 = \frac{-\gamma+\sqrt{\gamma^2-4}}{2\varepsilon}, \quad \lambda_2^0 = \frac{-\gamma-\sqrt{\gamma^2-4}}{2\varepsilon}, \quad \lambda_0 = \frac{-\gamma}{2\varepsilon}, \quad \beta_0 = \frac{\sqrt{4-\gamma^2}}{2\varepsilon}. \tag{2.12}$$

Solving the ODE (2.10) with the initial data (2.11), we get the dynamics of the mean value of the meson field when $v = 0$:

(i) for $\gamma > 2$

$$N(t) = D(0) + \frac{N(\phi^{(1)}) - \lambda_2^0(N(\phi^{(0)}) - D(0))}{\lambda_1^0 - \lambda_2^0}\mathrm{e}^{\lambda_1^0 t} + \frac{-N(\phi^{(1)}) + \lambda_1^0(N(\phi^{(0)}) - D(0))}{\lambda_1^0 - \lambda_2^0}\mathrm{e}^{\lambda_2^0 t};$$

(ii) for $\gamma = 2$

$$N(t) = D(0) + (N(\phi^{(0)}) - D(0))\mathrm{e}^{\lambda_0 t} + (N(\phi^{(1)}) - \lambda_0(N(\phi^{(0)}) - D(0)))t\mathrm{e}^{\lambda_0 t};$$

and

(iii) for $0 \leqslant \gamma < 2$

$$N(t) = D(0) + \mathrm{e}^{\lambda_0 t}\left[(N(\phi^{(0)}) - D(0))\cos(\beta_0 t) + \frac{N(\phi^{(1)}) - \lambda_0(N(\phi^{(0)}) - D(0))}{\beta_0}\sin(\beta_0 t)\right].$$

These immediately imply that $\lim_{t\to\infty} N(t) = D(0)$ when $\gamma > 0$, and $N(t)$ is a periodic function with period $T = 2\varepsilon\pi$ when $\gamma = 0$.

(f) *'Nonrelativistic' limit.* When $\varepsilon \to 0$ in (1.1), (1.2), corresponding to infinite speed of light, we get formally the well-known Schrödinger–Yukawa (S–Y) equations without ($v = 0$) or with ($v > 0$) a linear damping term:

$$\mathrm{i}\partial_t\psi + \Delta\psi + \phi\psi + \mathrm{i}v\psi = 0, \quad \mathbf{x} \in \mathbb{R}^d, \quad t > 0, \tag{2.13}$$

$$-\Delta\phi + \phi = |\psi|^2, \quad \mathbf{x} \in \mathbb{R}^d, \quad t > 0. \tag{2.14}$$

When $v = 0$, the S–Y equations (2.13) and (2.14) is time reversible, time transverse invariant, and preserves the following wave energy and Hamiltonian:

$$D^{\mathrm{SY}} = \int_{\mathbb{R}^d} |\psi(\mathbf{x},t)|^2\mathrm{d}\mathbf{x}, \tag{2.15}$$

$$H^{\mathrm{SY}} = \int_{\mathbb{R}^d}\left[\frac{1}{2}(\phi^2(\mathbf{x},t) + |\nabla\phi(\mathbf{x},t)|^2) + |\nabla\psi(\mathbf{x},t)|^2 - |\psi(\mathbf{x},t)|^2\phi(\mathbf{x},t)\right]\mathrm{d}\mathbf{x}. \tag{2.16}$$

Similarly, letting $\varepsilon \to 0$ in (2.2), we get formally the quadratic convergence rate of the Hamiltonian from KGS with $v = \gamma = 0$ to S–Y in the 'nonrelativistic' limit regime, i.e., $0 < \varepsilon \ll 1$:

$$H(t) = \int_{\mathbb{R}^d} \left[\frac{1}{2}(\phi^2(\mathbf{x},t) + |\nabla\phi(\mathbf{x},t)|^2) + |\nabla\psi(\mathbf{x},t)|^2 - |\psi(\mathbf{x},t)|^2\phi(\mathbf{x},t)\right]\mathrm{d}\mathbf{x} + \varepsilon^2 \int_{\mathbb{R}^d} (\partial_t\phi(\mathbf{x},t))^2\mathrm{d}\mathbf{x}$$
$$\approx H^{\mathrm{SY}} + \mathrm{O}(\varepsilon^2). \tag{2.17}$$

Our numerical results in Section 5 confirm this asymptotic result.

3. Numerical methods for the KGS equations

In this section, we present new efficient and accurate numerical methods for the KGS (1.1)–(1.3). For simplicity of notation, we shall introduce the method for KGS in 1D with periodic boundary conditions. Generalizations to higher dimensions are straightforward for tensor product grids and the results remain valid without modifications. For $d = 1$, the problem becomes

$$\mathrm{i}\partial_t\psi(x,t) + \partial_{xx}\psi + \mathrm{i}v\psi + \phi\psi = 0, \quad a < x < b, \quad t > 0, \tag{3.1}$$
$$\varepsilon^2\partial_{tt}\phi + \varepsilon\gamma\partial_t\phi - \partial_{xx}\phi + \phi - |\psi|^2 = 0, \quad a < x < b, \quad t > 0, \tag{3.2}$$
$$\psi(a,t) = \psi(b,t), \quad \partial_x\psi(a,t) = \partial_x\psi(b,t), \quad t \geqslant 0, \tag{3.3}$$
$$\phi(a,t) = \phi(b,t), \quad \partial_x\phi(a,t) = \partial_x\phi(b,t), \quad t \geqslant 0, \tag{3.4}$$
$$\psi(x,0) = \psi^{(0)}(x), \quad \phi(x,0) = \phi^{(0)}(x), \quad \partial_t\phi(x,0) = \phi^{(1)}(x), \quad a \leqslant x \leqslant b. \tag{3.5}$$

As is well known, the above KGS in 1D has the following properties:

$$D(t) = \int_a^b |\psi(x,t)|^2\mathrm{d}x = \mathrm{e}^{-2vt}\int_a^b |\psi^{(0)}(x)|^2\mathrm{d}x = \mathrm{e}^{-2vt}D(0), \quad t \geqslant 0. \tag{3.6}$$

So when $v = 0$, $D(t) \equiv D(0)$, i.e., it is an invariant of the KGS. When $v > 0$, it decays to 0 exponentially. Furthermore, when $v = 0$ and $\gamma = 0$, the KGS also conserves the Hamiltonian:

$$H(t) = \int_b^a \left[\frac{1}{2}(\phi(x,t)^2 + \varepsilon^2(\partial_t\phi(x,t))^2 + (\partial_x\phi(x,t))^2) + |\partial_x\psi(x,t)|^2 - |\psi(x,t)|^2\phi(x,t)\right]\mathrm{d}x \equiv H(0), \quad t \geqslant 0. \tag{3.7}$$

In some cases, the periodic boundary conditions (3.3) and (3.4) may be replaced by the homogeneous Dirichlet boundary conditions

$$\psi(a,t) = \psi(b,t) = 0, \quad \phi(a,t) = \phi(b,t) = 0, \quad t \geqslant 0. \tag{3.8}$$

We choose the spatial mesh size $h = \Delta x > 0$ with $h = (b-a)/M$ for M being an even positive integer, the time step size being $k = \Delta t > 0$ and let the grid points and the time steps be

$$x_j := a + jh, \quad j = 0, 1, \ldots, M; \quad t_m := mk, \quad m = 0, 1, 2, \ldots.$$

Let ψ_j^m and ϕ_j^m be the approximations of $\psi(x_j, t_m)$ and $\phi(x_j, t_m)$, respectively. Furthermore, let ψ^{m} and ϕ^m be the solution vector at time $t = t_m = mk$ with components ψ_j^m and ϕ_j^m, respectively.

From time $t = t_m$ to $t = t_{m+1}$, the first NLS-type equation (3.1) is solved in two splitting steps [1–3,36]. One solves first

$$\mathrm{i}\partial_t\psi + \partial_{xx}\psi = 0, \tag{3.9}$$

for the time step of length k, followed by solving

$$\mathrm{i}\partial_t\psi + \mathrm{i}v\psi + \phi\psi = 0, \tag{3.10}$$

for the same time step. Eq. (3.9) will be discretized in space by the Fourier spectral method and integrated in time *exactly*. For each fixed $x \in [a,b]$, integrating (3.10) from time $t = t_m$ to $t = t_{m+1} = t_m + k$, and then approximating the integral on $[t_m, t_{m+1}]$ via the trapezoidal rule [5,4], we obtain

$$\psi(x,t_{m+1}) = \exp\left[\int_{t_m}^{t_{m+1}} (-v + \mathrm{i}\phi(x,\tau))\mathrm{d}\tau\right]\psi(x,t_m)$$
$$= \exp\left[-vk + \mathrm{i}k\frac{\phi(x,t_m)+\phi(x,t_{m+1})}{2}\right]\psi(x,t_m), \quad a \leqslant x \leqslant b. \tag{3.11}$$

3.1. Phase space analytical solver + time-splitting spectral discretizations (PSAS–TSSP)

The Klein–Gordon equation (3.2) in KGS is discretized by using a pseudospectral method for spatial derivatives and then solving the ODEs in phase space analytically under appropriate chosen transmission conditions between different time intervals. From time $t = t_m$ to $t = t_{m+1}$, assume

$$\phi(x,t) = \sum_{l=-M/2}^{M/2-1} \tilde{\phi}_l^m(t)\mathrm{e}^{\mathrm{i}\mu_l(x-a)}, \quad a \leqslant x \leqslant b, \quad t_m \leqslant t \leqslant t_{m+1}, \tag{3.12}$$

where $\mu_l = \frac{2\pi l}{b-a}$ and $\tilde{\phi}_l^m(t)$ is the Fourier coefficient of the lth mode. Plugging (3.12) into (3.2) and noticing the orthogonality of the Fourier functions, we get the following ODEs:

$$\varepsilon^2\frac{\mathrm{d}^2\tilde{\phi}_l^m(t)}{\mathrm{d}t^2} + \varepsilon\gamma\frac{\mathrm{d}\tilde{\phi}_l^m(t)}{\mathrm{d}t} + (\mu_l^2+1)\tilde{\phi}_l^m(t) - \widetilde{\left(|\psi(t_m)|^2\right)}_l = 0, \quad t_m \leqslant t \leqslant t_{m+1}, \quad m \geqslant 0, \tag{3.13}$$

$$\tilde{\phi}_l^m(t_m) = \begin{cases} \widetilde{\left(\phi^{(0)}\right)}_l, & m = 0, \\ \tilde{\phi}_l^{m-1}(t_m), & m > 0, \end{cases} \quad l = -\frac{M}{2},\ldots,\frac{M}{2}-1. \tag{3.14}$$

For each fixed l $(-M/2 \leqslant l \leqslant M/2-1)$, Eq. (3.13) is a second-order ODE. It needs two initial conditions such that the solution is unique. When $m = 0$ in (3.13) and (3.14), we have the initial condition (3.14) and we can pose the other initial condition for (3.13) due to the initial condition (3.5):

$$\frac{\mathrm{d}}{\mathrm{d}t}\tilde{\phi}_l^0(t_0) = \frac{\mathrm{d}}{\mathrm{d}t}\tilde{\phi}_l^0(0) = \widetilde{\left(\phi^{(1)}\right)}_l, \quad l = -\frac{M}{2},\ldots,\frac{M}{2}-1. \tag{3.15}$$

Denote

$$\lambda_1 = \frac{-\gamma+\sqrt{\gamma^2-4(\mu_l^2+1)}}{2\varepsilon}, \quad \lambda_2 = \frac{-\gamma-\sqrt{\gamma^2-4(\mu_l^2+1)}}{2\varepsilon}, \quad \beta = \frac{\sqrt{4(\mu_l^2+1)-\gamma^2}}{2\varepsilon}. \tag{3.16}$$

Then the solution of (3.13), (3.14) with $m = 0$ and (3.15) for l $(-M/2 \leqslant l < M/2)$ and $0 \leqslant t \leqslant t_1$ is

(i) For $\gamma^2 - 4(\mu_l^2+1) > 0$

$$\tilde{\phi}_l^0(t) = \frac{\widetilde{\left(|\psi^{(0)}|^2\right)}_l}{\mu_l^2+1} + \frac{\varepsilon}{\sqrt{\gamma^2-4(\mu_l^2+1)}}\left[\widetilde{\left(\phi^{(1)}\right)}_l - \left(\widetilde{\left(\phi^{(0)}\right)}_l - \frac{\widetilde{\left(|\psi^{(0)}|^2\right)}_l}{\mu_l^2+1}\right)\lambda_2\right]\mathrm{e}^{\lambda_1 t}$$
$$- \frac{\varepsilon}{\sqrt{\gamma^2-4(\mu_l^2+1)}}\left[\widetilde{\left(\phi^{(1)}\right)}_l - \left(\widetilde{\left(\phi^{(0)}\right)}_l - \frac{\widetilde{\left(|\psi^{(0)}|^2\right)}_l}{\mu_l^2+1}\right)\lambda_1\right]\mathrm{e}^{\lambda_2 t}; \tag{3.17}$$

(ii) for $\gamma^2 - 4(\mu_l^2+1) = 0$,

$$\tilde{\phi}_l^0(t) = \frac{\widetilde{\left(|\psi^{(0)}|^2\right)}_l}{\mu_l^2+1} + \left[\widetilde{\left(\phi^{(0)}\right)}_l - \frac{\widetilde{\left(|\psi^{(0)}|^2\right)}_l}{\mu_l^2+1} + \left(\widetilde{\left(\phi^{(1)}\right)}_l + \frac{\gamma}{2\varepsilon}\left(\widetilde{\left(\phi^{(0)}\right)}_l - \frac{\widetilde{\left(|\psi^{(0)}|^2\right)}_l}{\mu_l^2+1}\right)\right)t\right]\mathrm{e}^{-\frac{\gamma t}{2\varepsilon}}; \tag{3.18}$$

and

(iii) for $\gamma^2 - 4(\mu_l^2+1) < 0$

$$\tilde{\phi}_l^0(t)=\mathrm{e}^{-\frac{\gamma t}{2\varepsilon}}\left[\frac{1}{\beta}\left(\widetilde{\left(\phi^{(1)}\right)}_l+\frac{\gamma}{2\varepsilon}\left(\widetilde{\left(\phi^{(0)}\right)}_l-\frac{\widetilde{\left(|\psi^{(0)}|^2\right)}_l}{\mu_l^2+1}\right)\right)\sin(\beta t)+\left(\widetilde{\left(\phi^{(0)}\right)}_l-\frac{\widetilde{\left(|\psi^{(0)}|^2\right)}_l}{\mu_l^2+1}\right)\cos(\beta t)\right]+\frac{\widetilde{\left(|\psi^{(0)}|^2\right)}_l}{\mu_l^2+1}. \tag{3.19}$$

But when $m>0$, we only have one initial condition (3.14). One cannot simply pose the continuity between $\frac{\mathrm{d}}{\mathrm{d}t}\tilde{\phi}_l^m(t)$ and $\frac{\mathrm{d}}{\mathrm{d}t}\tilde{\phi}_l^{m-1}(t)$ across the time $t=t_m$, because the last term in (3.13) is usually different in two adjacent time intervals $[t_{m-1},t_m]$ and $[t_m,t_{m+1}]$; i.e., $\widetilde{\left(|\psi(t_{m-1})|^2\right)}_l\neq\widetilde{\left(|\psi(t_m)|^2\right)}_l$. Since our goal is to develop an explicit scheme and we need to linearize the nonlinear term in (3.2) in our discretization (3.13), in general,

$$\frac{\mathrm{d}}{\mathrm{d}t}\tilde{\phi}_l^{m-1}(t_m^-)=\lim_{t\to t_m^-}\frac{\mathrm{d}}{\mathrm{d}t}\tilde{\phi}_l^{m-1}(t)\neq\lim_{t\to t_m^+}\frac{\mathrm{d}}{\mathrm{d}t}\tilde{\phi}_l^{m}(t)=\frac{\mathrm{d}}{\mathrm{d}t}\tilde{\phi}_l^{m}(t_m^+),\quad m=1,2,\ldots,\quad l=-\frac{M}{2},\ldots,\frac{M}{2}-1. \tag{3.20}$$

Unfortunately, we do not know the jump $\frac{\mathrm{d}}{\mathrm{d}t}\tilde{\phi}_l^m(t_m^+)-\frac{\mathrm{d}}{\mathrm{d}t}\tilde{\phi}_l^{m-1}(t_m^-)$ across the time $t=t_m$. In order to get a unique solution of (3.13) and (3.14) for $m>0$, we pose here an additional condition:

$$\tilde{\phi}_l^m(t_{m-1})=\tilde{\phi}_l^{m-1}(t_{m-1}),\quad l=-\frac{M}{2},\ldots,\frac{M}{2}-1. \tag{3.21}$$

Condition (3.21) is equivalent to posing that the solution $\tilde{\phi}_l^m(t)$ on the time interval $[t_m,t_{m+1}]$ of (3.13) and (3.14) is also continuous at the time $t=t_{m-1}$. After a simple computation, we get the solution of (3.13), (3.14) and (3.21) with $m>0$ for l $(l=-M/2,\ldots,M/2-1)$ and $t_m\leqslant t\leqslant t_{m+1}$:

(i) for $\gamma^2-4(\mu_l^2+1)>0$

$$\begin{aligned}\tilde{\phi}_l^m(t)=&\frac{1}{\mathrm{e}^{-k\lambda_1}-\mathrm{e}^{-k\lambda_2}}\left[\frac{\widetilde{\left(|\psi^m|^2\right)}_l}{\mu_l^2+1}(\mathrm{e}^{-k\lambda_2}-1)+\tilde{\phi}_l^{m-1}(t_{m-1})-\tilde{\phi}_l^{m-1}(t_m)\mathrm{e}^{-k\lambda_2}\right]\mathrm{e}^{\lambda_1(t-t_m)}\\&+\frac{1}{\mathrm{e}^{-k\lambda_2}-\mathrm{e}^{-k\lambda_1}}\left[\frac{\widetilde{\left(|\psi^m|^2\right)}_l}{\mu_l^2+1}(\mathrm{e}^{-k\lambda_1}-1)+\tilde{\phi}_l^{m-1}(t_{m-1})-\tilde{\phi}_l^{m-1}(t_m)\mathrm{e}^{-k\lambda_1}\right]\mathrm{e}^{\lambda_2(t-t_m)}+\frac{\widetilde{\left(|\psi^m|^2\right)}_l}{\mu_l^2+1};\end{aligned} \tag{3.22}$$

(ii) for $\gamma^2-4(\mu_l^2+1)=0$

$$\begin{aligned}\tilde{\phi}_l^m(t)=&\left[\frac{t-t_m}{k}\left(\tilde{\phi}_l^{m-1}(t_m)-\frac{\widetilde{\left(|\psi^m|^2\right)}_l}{\mu_l^2+1}+\mathrm{e}^{-\frac{k\gamma}{2\varepsilon}}\left(\frac{\widetilde{\left(|\psi^m|^2\right)}_l}{\mu_l^2+1}-\tilde{\phi}_l^{m-1}(t_{m-1})\right)\right)+\tilde{\phi}_l^{m-1}(t_m)-\frac{\widetilde{\left(|\psi^m|^2\right)}_l}{\mu_l^2+1}\right]\mathrm{e}^{-\frac{\gamma(t-t_m)}{2\varepsilon}}\\&+\frac{\widetilde{\left(|\psi^m|^2\right)}_l}{\mu_l^2+1};\end{aligned} \tag{3.23}$$

and

(iii) for $\gamma^2-4(\mu_l^2+1)<0$

$$\begin{aligned}\tilde{\phi}_l^m(t)=&\mathrm{e}^{-\frac{\gamma(t-t_m)}{2\varepsilon}}\left[\left(\tilde{\phi}_l^{m-1}(t_m)-\frac{\widetilde{\left(|\psi^m|^2\right)}_l}{\mu_l^2+1}\right)(\cos(\beta(t-t_m))+\cot(\beta k)\sin(\beta(t-t_m)))\right.\\&\left.+\mathrm{e}^{-\frac{\gamma k}{2\varepsilon}}\left(\frac{\widetilde{\left(|\psi^m|^2\right)}_l}{\mu_l^2+1}-\tilde{\phi}_l^{m-1}(t_{m-1})\right)\frac{\sin(\beta(t-t_m))}{\sin(\beta k)}\right]+\frac{\widetilde{\left(|\psi^m|^2\right)}_l}{\mu_l^2+1}.\end{aligned} \tag{3.24}$$

From time $t=t_m$ to $t=t_{m+1}$, we combine the splitting steps via the standard Strang splitting [35,1,3]:

$$\phi_j^{m+1} = \sum_{l=-M/2}^{M/2-1} (\widetilde{\phi^{m+1}})_l \mathrm{e}^{\mathrm{i}\mu_l(x_j-a)}, \tag{3.25}$$

$$\begin{aligned}
&\psi_j^* = \sum_{l=-M/2}^{M/2-1} \mathrm{e}^{-\mathrm{i}k\mu_l^2/2} (\widetilde{\psi^m})_l \mathrm{e}^{\mathrm{i}\mu_l(x_j-a)},\\
&\psi_j^{**} = \mathrm{e}^{-vk+ik(\phi_j^m+\phi_j^{m+1})/2}\psi_j^*,\\
&\psi_j^{m+1} = \sum_{l=-M/2}^{M/2-1} \mathrm{e}^{-\mathrm{i}k\mu_l^2/2} (\widetilde{\psi^{**}})_l \mathrm{e}^{\mathrm{i}\mu_l(x_j-a)}, \quad 0 \leqslant j \leqslant M-1, \quad m \geqslant 0;
\end{aligned} \tag{3.26}$$

where $\widetilde{U_l}$, the Fourier coefficients of a vector $U = (U_0, U_1, U_2, \ldots, U_M)^{\mathrm{T}}$ with $U_0 = U_M$, are defined as

$$\widetilde{U_l} = \frac{1}{M}\sum_{j=0}^{M-1} U_j \mathrm{e}^{-\mathrm{i}\mu_l(x_j-a)}, \quad l = -\frac{M}{2}, \ldots, \frac{M}{2}-1, \tag{3.27}$$

and

(i) for $\gamma^2 - 4(\mu_l^2+1) > 0$

$$\left(\widetilde{\phi^{m+1}}\right)_l = \begin{cases}
\frac{\varepsilon(\mathrm{e}^{\lambda_1 k}-\mathrm{e}^{\lambda_2 k})}{\sqrt{\gamma^2-4(\mu_l^2+1)}}\left(\widetilde{\phi^{(1)}}\right)_l + \frac{\varepsilon(\lambda_1\mathrm{e}^{\lambda_2 k}-\lambda_2\mathrm{e}^{\lambda_1 k})}{\sqrt{\gamma^2-4(\mu_l^2+1)}}\left(\widetilde{\phi^{(0)}}\right)_l\\
+\left(\frac{\varepsilon\left(\lambda_2\mathrm{e}^{\lambda_1 k}-\lambda_1\mathrm{e}^{\lambda_2 k}\right)}{\sqrt{\gamma^2-4(\mu_l^2+1)}}+1\right)\frac{\left(\widetilde{|\psi^{(0)}|^2}\right)_l}{\mu_l^2+1}, \quad m = 0,\\
-\mathrm{e}^{(\lambda_1+\lambda_2)k}\left(\widetilde{\phi^{m-1}}\right)_l + (\mathrm{e}^{\lambda_1 k}+\mathrm{e}^{\lambda_2 k})(\widetilde{\phi^m})_l\\
+(\mathrm{e}^{\lambda_1 k}-1)(\mathrm{e}^{\lambda_2 k}-1)\frac{\left(\widetilde{|\psi^m|^2}\right)_l}{\mu_l^2+1}, \quad m \geqslant 1;
\end{cases} \tag{3.28}$$

(ii) for $\gamma^2 - 4(\mu_l^2+1) = 0$

$$\left(\widetilde{\phi^{m+1}}\right)_l = \begin{cases}
\left(1+\frac{\gamma k}{2\varepsilon}\right)\mathrm{e}^{-\frac{\gamma k}{2\varepsilon}}\left(\widetilde{\phi^{(0)}}\right)_l + k\mathrm{e}^{-\frac{\gamma k}{2\varepsilon}}\left(\widetilde{\phi^{(1)}}\right)_l\\
-\left(\left(1+\frac{\gamma k}{2\varepsilon}\right)\mathrm{e}^{-\frac{\gamma k}{2\varepsilon}}-1\right)\frac{\left(\widetilde{|\psi^{(0)}|^2}\right)_l}{\mu_l^2+1}, \quad m = 0,\\
2\mathrm{e}^{-\frac{k\gamma}{2\varepsilon}}(\widetilde{\phi^m})_l - \mathrm{e}^{-\frac{\gamma k}{\varepsilon}}\left(\widetilde{\phi^{m-1}}\right)_l\\
+\left(\mathrm{e}^{-\frac{\gamma k}{2\varepsilon}}-1\right)^2\frac{\left(\widetilde{|\psi^m|^2}\right)_l}{\mu_l^2+1}, \quad m \geqslant 1;
\end{cases} \tag{3.29}$$

and

(iii) for $\gamma^2 - 4(\mu_l^2+1) < 0$

$$\left(\widetilde{\phi^{m+1}}\right)_l = \begin{cases}
\left(\cos(\beta k)+\frac{\gamma}{2\beta\varepsilon}\sin(\beta k)\right)\mathrm{e}^{-\frac{\gamma k}{2\varepsilon}}\left(\widetilde{\phi^{(0)}}\right)_l + \frac{\sin(\beta k)}{\beta}\mathrm{e}^{-\frac{\gamma k}{2\varepsilon}}\left(\widetilde{\phi^{(1)}}\right)_l\\
-\left(\left(\cos(\beta k)+\frac{\gamma}{2\beta\varepsilon}\sin(\beta k)\right)\mathrm{e}^{-\frac{\gamma k}{2\varepsilon}}-1\right)\frac{\left(\widetilde{|\psi^{(0)}|^2}\right)_l}{\mu_l^2+1}, & m = 0,\\
-\mathrm{e}^{-\frac{\gamma k}{\varepsilon}}\left(\widetilde{\phi^{m-1}}\right)_l + 2\cos(\beta k)\mathrm{e}^{-\frac{\gamma k}{2\varepsilon}}(\widetilde{\phi^m})_l\\
-\left(2\cos(\beta k)\mathrm{e}^{-\frac{\gamma k}{2\varepsilon}}-\mathrm{e}^{-\frac{\gamma k}{\varepsilon}}-1\right)\frac{\left(\widetilde{|\psi^m|^2}\right)_l}{\mu_l^2+1}, & m \geqslant 1.
\end{cases} \tag{3.30}$$

The initial conditions (3.5) are discretized as

$$\psi_j^0 = \psi^{(0)}(x_j), \quad \phi_j^0 = \phi^{(0)}(x_j), \quad \phi_j^{(1)} = \phi^{(1)}(x_j), \quad 0 \leqslant j \leqslant M. \tag{3.31}$$

Note that the spatial discretization error of the above method is of spectral order accuracy in h, and the time discretization error is demonstrated to be of second-order accuracy in k in Section 5 from our numerical results.

3.2. Crank–Nicolson leap-frog time-splitting spectral discretizations (CN–LF–TSSP)

Another way to discretize the Klein–Gordon equation (3.2) in the KGS is by using a pseudospectral method for spatial derivatives, followed by application of a Crank–Nicolson/leap-frog method for linear/nonlinear terms for time derivatives:

$$\varepsilon^2\frac{\phi_j^{m+1}-2\phi_j^m+\phi_j^{m-1}}{k^2}+\varepsilon\gamma\frac{\phi_j^{m+1}-\phi_j^{m-1}}{2k}-D_{xx}^f(\beta\phi^{m+1}+(1-2\beta)\phi^m+\beta\phi^{m-1})_{x=x_j}$$
$$+(\beta\phi_j^{m+1}+(1-2\beta)\phi_j^m+\beta\phi_j^{m-1})-|\psi_j^m|^2=0,\quad 0\leqslant j\leqslant M,\quad m\geqslant 0, \tag{3.32}$$

where $0\leqslant\beta\leqslant 1/2$ is a constant; D_{xx}^f, a spectral differential operator approximation of ∂_{xx}, is defined as

$$D_{xx}^f U|_{x=x_j}=-\sum_{l=-M/2}^{M/2-1}\mu_l^2\widetilde{U}_l e^{i\mu_l(x_j-a)}. \tag{3.33}$$

When $\beta=0$ in (3.32), the discretization (3.32) to the Eq. (3.2) is *explicit*. When $0<\beta\leqslant 1/2$, the discretization is *implicit*, but can be solved *explicitly*. In fact, suppose

$$\phi_j^m=\sum_{l=-M/2}^{M/2-1}(\widetilde{\phi^m})_l e^{i\mu_l(x_j-a)},\quad j=0,\ldots,M,\quad m=0,1,\ldots. \tag{3.34}$$

Plugging (3.34) into (3.32) and using the orthogonality of the Fourier functions, we obtain for $m\geqslant 1$

$$\varepsilon^2\frac{(\widetilde{\phi^{m+1}})_l-2(\widetilde{\phi^m})_l+(\widetilde{\phi^{m-1}})_l}{k^2}+\varepsilon\gamma\frac{(\widetilde{\phi^{m+1}})_l-(\widetilde{\phi^{m-1}})_l}{2k}-\left(\widetilde{|\psi^m|^2}\right)_l+(\mu_l^2+1)(\beta(\widetilde{\phi^{m+1}})_l$$
$$+(1-2\beta)(\widetilde{\phi^m})_l+\beta(\widetilde{\phi^{m-1}})_l)=0,\quad 0\leqslant j\leqslant M. \tag{3.35}$$

Solving the above equation, we get

$$(\widetilde{\phi^{m+1}})_l=\frac{4\varepsilon^2+2(2\beta-1)(\mu_l^2+1)k^2}{2k^2\beta(\mu_l^2+1)+\varepsilon\gamma k+2\varepsilon^2}(\widetilde{\phi^m})_l-\left(1-\frac{2\varepsilon\gamma k}{2k^2\beta(\mu_l^2+1)+\varepsilon\gamma k+2\varepsilon^2}\right)(\widetilde{\phi^{m-1}})_l$$
$$+\frac{2k^2}{2k^2\beta(\mu_l^2+1)+\varepsilon\gamma k+2\varepsilon^2}\left(\widetilde{|\psi^m|^2}\right)_l,\quad -\frac{M}{2}\leqslant l<\frac{M}{2},\quad m\geqslant 1. \tag{3.36}$$

From time $t=t_m$ to $t=t_{m+1}$, we combine the splitting steps via the standard Strang splitting [35,1,3]:

$$\phi_j^{m+1}=\sum_{l=-M/2}^{M/2-1}(\widetilde{\phi^{m+1}})_l e^{i\mu_l(x_j-a)}, \tag{3.37}$$

$$\psi_j^*=\sum_{l=-M/2}^{M/2-1}e^{-ik\mu_l^2/2}(\widetilde{\psi^m})_l e^{i\mu_l(x_j-a)},$$
$$\psi_j^{**}=e^{-vk+ik(\phi_j^m+\phi_j^{m+1})/2}\psi_j^*$$
$$\psi_j^{m+1}=\sum_{l=-M/2}^{M/2-1}e^{-ik\mu_l^2/2}(\widetilde{\psi^{**}})_l e^{i\mu_l(x_j-a)},\quad 0\leqslant j\leqslant M-1,\quad m\geqslant 0. \tag{3.38}$$

The initial conditions are discretized as

$$\psi_j^0 = \psi^{(0)}(x_j), \quad \phi_j^0 = \phi^{(0)}(x_j), \quad \frac{\phi_j^1 - \phi_j^{-1}}{2k} = \phi^{(1)}(x_j), \quad 0 \leqslant j \leqslant M-1. \tag{3.39}$$

This implies that

$$\widetilde{(\phi^1)}_l = \frac{2\varepsilon^2 + (2\beta-1)(\mu_l^2+1)k^2}{2(\varepsilon^2+\beta(\mu_l^2+1)k^2)}\widetilde{(\phi^{(0)})}_l + \frac{k(2k^2\beta(\mu_l^2+1) - \varepsilon\gamma k + 2\varepsilon^2)}{2(\varepsilon^2+\beta(\mu_l^2+1)k^2)}\widetilde{(\phi^{(1)})}_l + \frac{k^2}{2(\varepsilon^2+\beta(\mu_l^2+1)k^2)}\widetilde{(|\psi^{(0)}|^2)}_l. \tag{3.40}$$

Note that the spatial discretization error of the method is of spectral order accuracy in h and the time discretization error is demonstrated to be second-order accurate in k in Section 5 from our numerical results.

4. Properties of the numerical methods

In this section, we will study properties of our new numerical methods for KGS, which are the discretized version of those reviewed in Section 2. Define the usual l^2-norm and mean value of a vector $U = (U_0, U_1, \ldots, U_M)^{\mathrm{T}}$ which is a discretization of a periodic function $U(x)$ on the interval $[a,b]$ with $U_j = U(x_j)$ $(j = 0,1,\ldots,M)$ as

$$\|U\|_{l^2} = \sqrt{\frac{b-a}{M}\sum_{j=0}^{M-1}|U_j|^2}, \quad N(U) = \frac{b-a}{M}\sum_{j=0}^{M-1}U_j. \tag{4.1}$$

(a) *Time reversible and time transverse invariant*. When $v = 0$ and $\gamma = 0$, the numerical methods PSAS–TSSP (3.25)–(3.26) and CN–LF–TSSP (3.37)–(3.38) are time reversible, i.e. they are unchanged if we interchange $m+1 \leftrightarrow m-1$ and $k \leftrightarrow -k$. Furthermore, the PSAS–TSSP (3.25) and (3.26) is time transverse invariant. If constants α and β are added to the initial data $\phi^{(0)}(x_j)$ and $\phi^{(1)}(x_j)$ in (3.5), respectively, i.e. $\phi^{(0)}(x_j) \to \phi^{(0)}(x_j) + \alpha$ and $\phi^{(1)}(x_j) + \beta$, then the solution ϕ_j^m and ψ_j^m obtained from (3.25)–(3.26) get added by $\alpha\cos(t_m/\varepsilon) + \beta\varepsilon\sin(t_m/\varepsilon)$ and multiplied by $\mathrm{e}^{\mathrm{i}\varepsilon(\alpha\sin(t_m/\varepsilon)-\beta\varepsilon\cos(t_m/\varepsilon))}$, respectively, i.e. $\phi_j^m \to \phi_j^m + \alpha\cos(t_m/\varepsilon) + \beta\varepsilon\sin(t_m/\varepsilon)$ and $\psi_j^m \to \psi_j^m \mathrm{e}^{\mathrm{i}\varepsilon(\alpha\sin(t_m/\varepsilon)-\beta\varepsilon\cos(t_m/\varepsilon))}$, which leaves the wave energy density $|\psi_j^m|^2$ unchanged. This property is *not* kept by the finite difference method [41,25,10] and the spectral method [40,38] used for KGS in the literature.

(b) *Plane-wave solution in 1D*. When $d = 1$, $\varepsilon = 1$, $\gamma = 0$ and $v = 0$ in (3.1)–(3.5) and the initial data (3.5) is chosen as (2.5), the KGS in 1D admits the plane-wave solution (2.6). It is easy to see that in this case our numerical methods PSAS–TSSP (3.25)–(3.26) and CN–LF–TSSP (3.37)–(3.38) give exact results, provided that $M \geqslant 2(|l|+1)$.

(c) *Dynamics of the wave energy*. For the discretizations (3.25)–(3.26) and (3.37)–(3.38), we have the following result for dynamics of wave energy in discretized level:

Theorem 4.1. *The discretizations PSAS–TSSP (3.25)–(3.26) and CN–LF–TSSP (3.37)–(3.38) for KGS possess the following properties*:

$$\|\psi^m\|_{l^2}^2 = \mathrm{e}^{-2vt_m}\|\psi^0\|_{l^2}^2 = \mathrm{e}^{-2vt_m}\|\psi^{(0)}\|_{l^2}^2, \quad m = 0,1,2,\ldots. \tag{4.2}$$

Proof. Follow the line of the analogous results for the damped NLS [1] and the Zakharov system [5] by a time-splitting spectral method. □

(d) *Dynamics of the mean value of the meson filed when v = 0*. When $v = 0$, for the discretization PSAS–TSSP (3.25)–(3.26), we have the following results for the dynamics of the mean value of the meson field in discretized level:

Theorem 4.2. *When* $v = 0$, *the discretization PSAS–TSSP (3.25)–(3.26) for KGS possesses the following property*:

(*i*) *when* $\gamma > 2$

$$N(\phi^{m+1}) = D(0) + \frac{N(\phi^{(1)}) - \lambda_2^0(N(\phi^{(0)}) - D(0))}{\lambda_1^0 - \lambda_2^0} e^{\lambda_1^0 t_{m+1}} + \frac{-N(\phi^{(1)}) + \lambda_1^0(N(\phi^{(0)}) - D(0))}{\lambda_1^0 - \lambda_2^0} e^{\lambda_2^0 t_{m+1}}; \tag{4.3}$$

(*ii*) *when* $\gamma = 2$

$$N(\phi^{m+1}) = D(0) + (N(\phi^{(0)}) - D(0)) e^{\lambda_0 t_{m+1}} + (N(\phi^{(1)}) - \lambda_0(N(\phi^{(0)}) - D(0))) t_{m+1} e^{\lambda_0 t_{m+1}}; \tag{4.4}$$

and

(*iii*) *when* $0 \leqslant \gamma < 2$

$$N(\phi^{m+1}) = D(0) + e^{\lambda_0 t_{m+1}} \left[(N(\phi^{(0)}) - D(0)) \cos(\beta_0 t_{m+1}) + \frac{N(\phi^{(1)}) - \lambda_0(N(\phi^{(0)}) - D(0))}{\beta_0} \sin(\beta_0 t_{m+1}) \right]; \tag{4.5}$$

where

$$D(0) = N(|\psi_0|^2) = \frac{b-a}{M} \sum_{j=0}^{M-1} |\psi^{(0)}(x_j)|^2. \tag{4.6}$$

Proof. See Appendix A. □

(e) *Unconditional stability*. By using the standard von Neumann analysis for the discretizetion PSAS–TSSP (3.25)–(3.26) and CN–LP–TSSP (3.37)–(3.38), we have

Theorem 4.3. *The discretization PSAS–TSSP (3.25)–(3.26) is unconditionally stable for any parameter value* $\gamma \geqslant 0$, *time step* $k > 0$ *and mesh size* $h > 0$. *When* $1/4 \leqslant \beta \leqslant 1/2$ *and* $\gamma = 0$, *the discretization CN–LP–TSSP (3.37)–(3.38) is unconditionally stable*; *and when* $0 \leqslant \beta < 1/4$ *and* $\gamma = 0$, *it is conditionally stable under the stability condition*

$$k \leqslant \frac{2h\varepsilon}{\sqrt{(1-4\beta)(\pi^2 + h^2)}}. \tag{4.7}$$

Proof. See Appendix B. □

5. Numerical examples

In this section, we will first test accuracy of our new numerical methods for KGS, then apply them to study solitary-wave interactions in 1D, and finally present a 2D example to demonstrate the efficiency and high accuracy of our numerical methods for KGS.

In all examples except for the plane wave, the initial data for (3.5) are always chosen such that $\psi^{(0)}$, $\phi^{(0)}$ and $\phi^{(1)}$ decay to zero sufficiently fast as $|\mathbf{x}|t \to \infty$. We always compute on a domain, which is large enough such that the periodic boundary conditions (3.8) do not introduce a significant aliasing error relative to the problem in the whole space.

5.1. Accuracy test of our numerical methods

Example 1. The standard KGS with a solitary wave solution in 1D, i.e., we choose $d = 1$ and $v = 0$ in (1.1)–(1.3). The initial data in (1.3) is chosen as

$$\psi^{(0)}(x) = \psi_+(\mathbf{x}, t = 0), \phi^{(0)}(x) = \phi_+(x, t = 0), \quad \phi^{(1)}(x) = \partial_t \phi_+(x, t = 0), \quad x \in \mathbb{R}; \tag{5.1}$$

where ψ_+ and ϕ_+ are given in (2.7), (2.8). In our computation, we take $B = 1$ in (2.7), (2.8) and solve the problem on the interval $[-32, 32]$, i.e., $a = -32$ and $b = 32$ with periodic boundary conditions. When $\gamma = 0$, the KGS admits the well-known solitary wave solution (2.7)–(2.8) as exact solution. When $\gamma > 0$, there is no analytical solution and we let ψ and ϕ be the 'exact' solutions which are obtained numerically by using our numerical method with a very fine mesh and small time step size, e.g. $h = \frac{1}{32}$ and $k = 0.0001$. Let $\psi_{h,k}$ and $\phi_{h,k}$ be the numerical solution obtained by using our method with mesh size h and time step k.

We present computations for two different regimes of the speed of light, i.e., $1/\varepsilon$.

Case I. O(1)-speed of light, i.e. we choose $\varepsilon = 1$ in (1.3) and (2.7)–(2.8). Here, we test the spatial and temporal discretization errors, conservation of the conserved quantities. To quantify the numerical results, we define the error functions as

$$e_1(t) = \|\psi(\cdot,t) - \psi_{h,k}(t)\|_{l^2}, \quad e_2(t) = \|\phi(\cdot,t) - \phi_{h,k}(t)\|_{l^2},$$
$$e(t) = \frac{\|\psi(\cdot,t) - \psi_{h,k}(t)\|_{l^2}}{\|\psi(\cdot,t)\|_{l^2}} + \frac{\|\phi(\cdot,t) - \phi_{h,k}(t)\|_{l^2}}{\|\phi(\cdot,t)\|_{l^2}} = \frac{e_1(t)}{\|\psi(\cdot,t)\|_{l^2}} + \frac{e_2(t)}{\|\phi(\cdot,t)\|_{l^2}}.$$

First, we test the discretization error in space. In order to do this, we choose a very small time step, e.g., $k = 0.0001$, such that the error from time discretization is negligible compared to the spatial discretization error, and solve the KGS with different methods under different mesh size h and γ. Table 1 lists the numerical errors of $e_1(t)$ and $e_2(t)$ at $t = 2$ with different mesh sizes h and parameter values γ for different numerical methods.Second, we test the discretization error in time. Table 2 shows the numerical errors $e_1(t)$ and $e_2(t)$ at $t = 1.0$ under different time steps k and mesh sizes h for different numerical methods.Third, we test the conservation of the conserved quantities. Table 3 presents the quantities and numerical errors at different times with mesh size $h = \frac{1}{8}$ and time step $k = 0.0001$ for different numerical methods.

Case II. "Nonrelativistic' limit regime, i.e. $0 < \varepsilon \ll 1$. We take $\gamma = 0$ in (1.2). Here we test the ε-resolution for different methods when $\varepsilon \to 0$. Two types of initial data are chosen:

- *Type 1*. O(ε)-wavelength in the initial data, i.e. we choose the initial data as in (5.1) with ε.
- *Type 2*. Well-prepared initial data with O(1)-wavelength, i.e., we choose the initial data as

Table 1
Spatial discretization errors $e_1(t)$ and $e_2(t)$ at time $t = 2$ for different mesh sizes h under $k = 0.0001$. I: For $\gamma = 0$ (upper 4 rows); II: for $\gamma = 0.5$ (lower 4 rows)

	Mesh	$h = 1.0$	$h = 1/2$	$h = 1/4$
PSAS–TSSP	e_1	1.341	5.031E − 3	9.006E − 8
	e_2	1.056	8.342E − 3	7.476E − 7
CN–LF–TSSP	e_1	1.341	5.031E − 3	8.418E − 7
	e_2	1.056	8.342E − 3	7.491E − 7
CN–LF–TSSP	e_1	1.341	5.031E − 3	9.327E − 8
	e_2	1.056	8.342E − 3	7.510E − 7
CN–LF–TSSP	e_1	1.341	5.081E − 3	1.140E − 7
	e_2	1.056	8.342E − 3	7.587E − 7
PSAS–TSSP	e_1	0.823	4.094E − 3	1.127E − 6
	e_2	0.715	3.324E − 3	1.729E − 6
CN–LF–TSSP	e_1	0.823	4.094E − 3	1.612E − 6
	e_2	0.715	3.324E − 3	1.078E − 6
CN–LF–TSSP	e_1	0.823	4.094E − 3	1.625E − 6
	e_2	0.715	3.324E − 3	1.105E − 6
CN–LF–TSSP	e_1	0.823	4.094E − 3	1.622E − 6
	e_2	0.715	3.324E − 3	1.120E − 6

Table 2
Temporal discretization errors $e_1(t)$ and $e_2(t)$ at time $t = 1$ for different time steps k. I: For $\gamma = 0$ (upper 4 rows); II: for $\gamma = 0.5$ and $h = 1/4$ (lower 4 rows)

	h	Error	$k = \frac{1}{25}$	$k = \frac{1}{100}$	$k = \frac{1}{400}$	$k = \frac{1}{1600}$
PSAS–TSSP	$\frac{1}{4}$	e_1	7.414E − 3	4.728E − 4	2.971E − 5	1.861E − 6
		e_2	2.409E − 3	1.538E − 4	9.681E − 6	7.421E − 7
	$\frac{1}{8}$	e_1	7.414E − 3	4.728E − 4	2.971E − 5	1.859E − 6
		e_2	2.409E − 3	1.538E − 4	9.672E − 6	6.054E − 7
CN–LF–TSSP ($\beta = 0$)	$\frac{1}{4}$	e_1	7.935E − 3	5.067E − 4	3.185E − 5	1.995E − 6
		e_2	7.882E − 4	5.086E − 5	3.242E − 5	4.738E − 7
	$\frac{1}{8}$	e_1	7.935E − 3	5.067E − 4	3.185E − 5	1.993E − 6
		e_2	7.882E − 4	5.086E − 5	3.212E − 6	2.013E − 7
CN–LF–TSSP ($\beta = 1/4$)	$\frac{1}{4}$	e_1	6.714E − 3	4.269E − 4	2.681E − 5	1.680E − 6
		e_2	5.690E − 3	3.622E − 4	2.275E − 5	1.486E − 6
	$\frac{1}{8}$	e_1	6.714E − 3	4.269E − 4	2.681E − 5	1.678E − 6
		e_2	5.690E − 3	3.622E − 4	2.274E − 5	1.423E − 6
CN–LF–TSSP ($\beta = 1/2$)	$\frac{1}{4}$	e_1	6.737E − 3	4.284E − 4	2.690E − 5	1.685E − 6
		e_2	1.061E − 2	6.752E − 4	4.237E − 5	2.686E − 6
	$\frac{1}{8}$	e_1	6.737E − 3	4.284E − 4	2.690E − 5	1.683E − 6
		e_2	1.061E − 2	6.752E − 4	4.237E − 5	2.651E − 6
	Error	$k = \frac{1}{4}$	$k = \frac{1}{8}$	$k = \frac{1}{16}$	$k = \frac{1}{32}$	$k = \frac{1}{64}$
PSAS–TSSP	e_1	4.135E − 1	7.965E − 2	1.885E − 2	4.694E − 3	1.173E − 3
	e_2	9.913E − 2	2.287E − 2	5.500E − 3	1.364E − 3	3.402E − 4
CN–LF–TSSP ($\beta = 0$)	e_1	3.948E − 1	7.120E − 2	1.656E − 2	4.117E − 3	1.028E − 3
	e_2	5.475E − 2	1.246E − 2	2.957E − 3	7.322E − 4	1.827e-4
CN–LF–TSSP ($\beta = 1/4$)	e_1	3.848E − 1	5.956E − 2	1.321E − 2	3.272E − 3	8.166E − 4
	e_2	2.058E − 1	5.011E − 2	1.235E − 2	3.079E − 3	7.690E − 4
CN–LF–TSSP ($\beta = 1/2$)	e_1	3.966E − 1	5.948E − 2	1.323E − 2	3.283E − 3	8.16E − 4
	e_2	3.517E − 1	8.874E − 2	2.216E − 2	5.541E − 3	1.385E − 3

Table 3
Conserved quantities analysis: $k = 0.0001$ and $h = \frac{1}{8}$

	Time	e	D	H
PSAS–TSSP	1.0	1.690E − 8	12.0000000	11.7286127
	2.0	2.672E − 8	12.0000000	11.7286128
CN–LF–TSSP $\beta = 0$	1.0	6.556E − 9	12.0000000	11.7286127
	2.0	2.211E − 8	12.0000000	11.7286128
CN–LF–TSSP $\beta = 1/4$	1.0	2.163E − 8	12.0000000	11.7286127
	2.0	4.342E − 8	12.0000000	11.7286128
CN–LF–TSSP $\beta = 1/2$	1.0	2.473E − 8	12.0000000	11.7286127
	2.0	4.815E − 8	12.0000000	11.7286128

$$\psi(x,0) = \psi^{(0)}(x) = \operatorname{sech}(x+p)\mathrm{e}^{-2\mathrm{i}(x+p)} + \operatorname{sech}(x-p)\mathrm{e}^{-2\mathrm{i}(x-p)}, \tag{5.2}$$

$$\phi(x,0) = \phi^{(0)}(x), \quad \partial_t\phi(x,0) = 0, \quad -\infty < x < \infty, \tag{5.3}$$

where $\phi^{(0)}$ satisfies

$$-\phi^{(0)}_{xx}(x) + \phi^{(0)}(x) = |\psi^{(0)}(x)|^2, \quad -\infty < x < \infty. \tag{5.4}$$

This kind of initial data for the KGS (1.1)–(1.2) is compatible with the initial data for its limiting S–Y equations (2.13)–(2.14).

We take $p = 8$ in (5.2). Fig. 1 shows the numerical results of PSAS–TSSP at $t = 1$ when we choose the meshing strategy $h = \mathrm{O}(\varepsilon)$ and $k = \mathrm{O}(\varepsilon)$: $\mathscr{T}_0 = (\varepsilon_0, h_0, k_0) = (0.125, 0.25, 0.04), \mathscr{T}_0/4, \mathscr{T}_0/16$; and $h = \mathrm{O}(\varepsilon)$ and $k = 0.04$-independent of ε: $\mathscr{T}_0 = (\varepsilon_0, h_0) = (0.125, 0.25), \mathscr{T}_0/4, \mathscr{T}_0/16$ for Type 1 initial data; and Fig. 2 shows similar results for Type 2 initial data. In addition, CN–LF–TSSP with $\beta = 1/4$ or $1/2$ gives similar numerical results at the same meshing strategies.

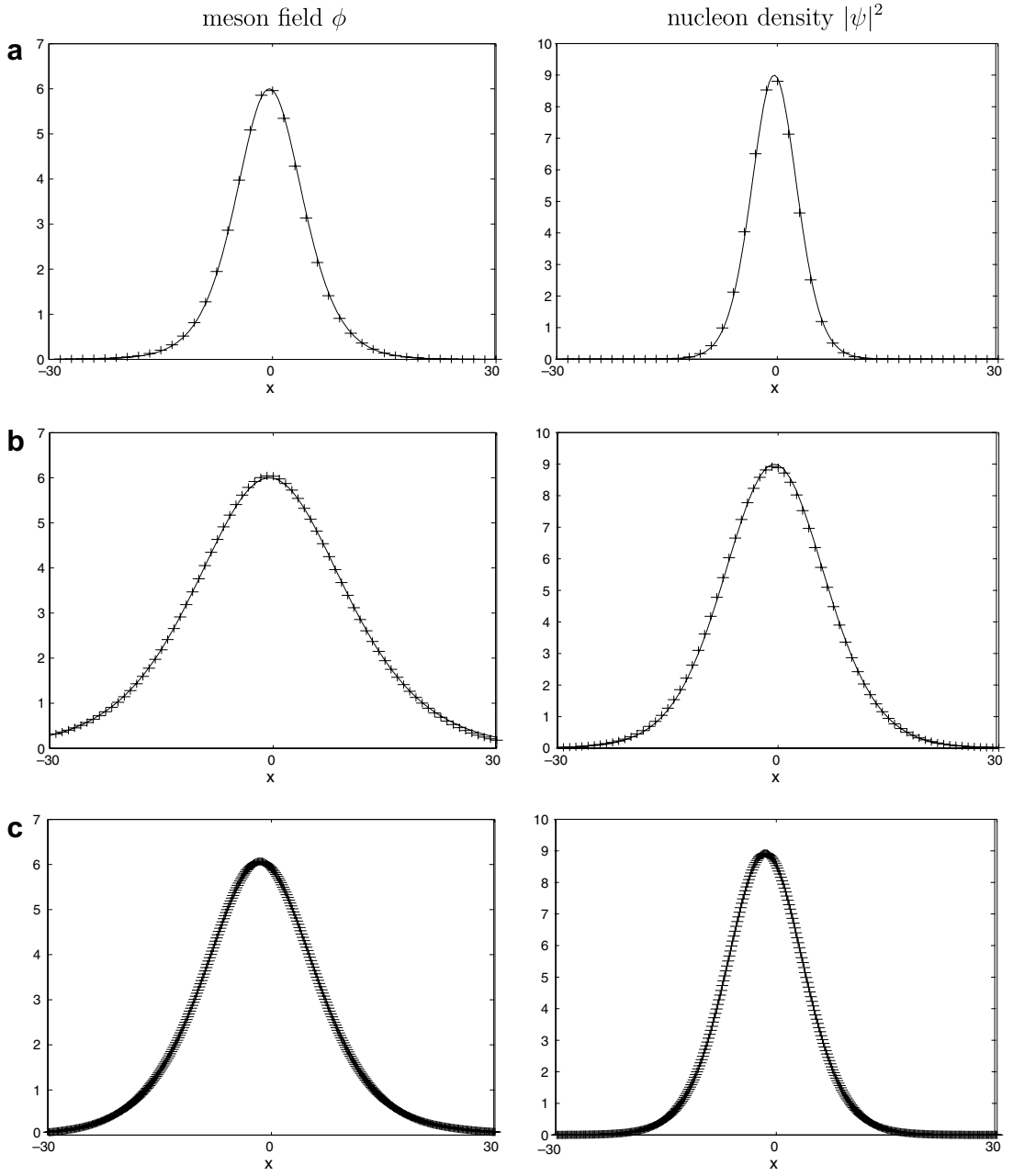

Fig. 1. Numerical solutions at $t = 1$ for Example 1 with Type 1 initial data in the 'nonrelativistic' limit regime by PSAS–TSSP. '−': exact solution given in (2.7), (2.8), '+++': numerical solution. I. With the meshing strategy $h = \mathrm{O}(\varepsilon)$ and $k = \mathrm{O}(\varepsilon)$: (a) $\mathscr{T}_0 = (\varepsilon_0, h_0, k_0) = (0.125, 0.25, 0.04)$, (b) $\mathscr{T}_0/4$, and (c) $\mathscr{T}_0/16$ ('this figure'); II. with the meshing strategy $h = \mathrm{O}(\varepsilon)$ and $k = 0.04$-independent of ε: (d) $\mathscr{T}_0 = (\varepsilon_0, h_0) = (0.125, 0.25)$, (e) $\mathscr{T}_0/4$, and (f) $\mathscr{T}_0/16$ ('continued').

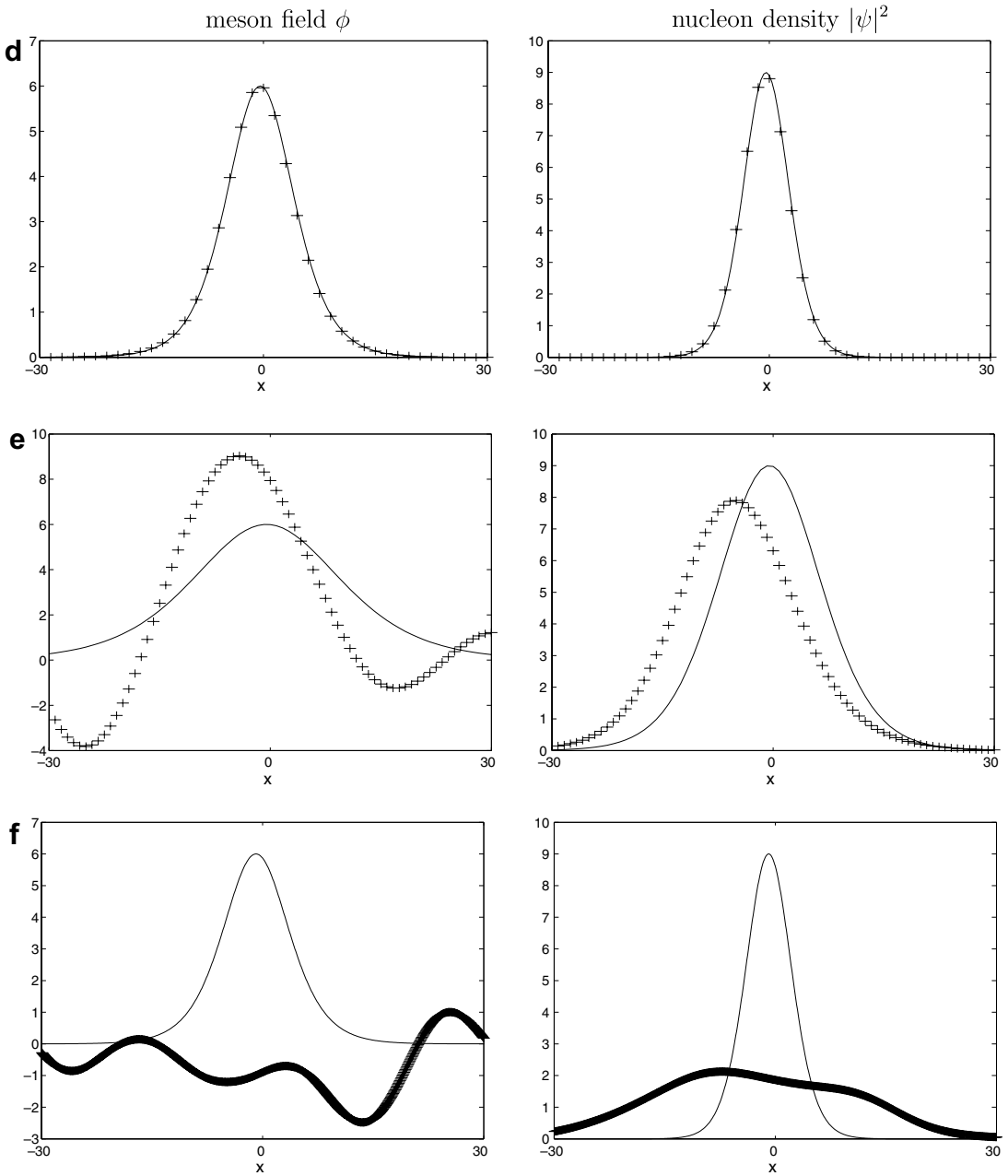

Fig. 1 (*continued*)

From Tables 1–3 and Figs. 1, 2, we can draw the following observations:

(i) In O(1)-speed of light regime, i.e. $\varepsilon = O(1)$ fixed, our new numerical methods PSAS–TSSP and CN–LF–TSSP are of spectral-order accuracy in space discretization and second-order accuracy in time. Moreover, PSAS–TSSP and CN–LP–TSSP with $\beta = 1/2$ or $\beta = 1/4$ are unconditionally stable, where CN–LP–TSSP with $\beta = 0$ is conditionally stable. Both numerical methods conserve the wave energy D exactly and the Hamiltonian H very well (up to eight significant digits). Furthermore, these two methods are explicit, easy to program, less memory requirement, easy to extend to 2D and 3D cases, and keep most properties of KGS in the discretized level.

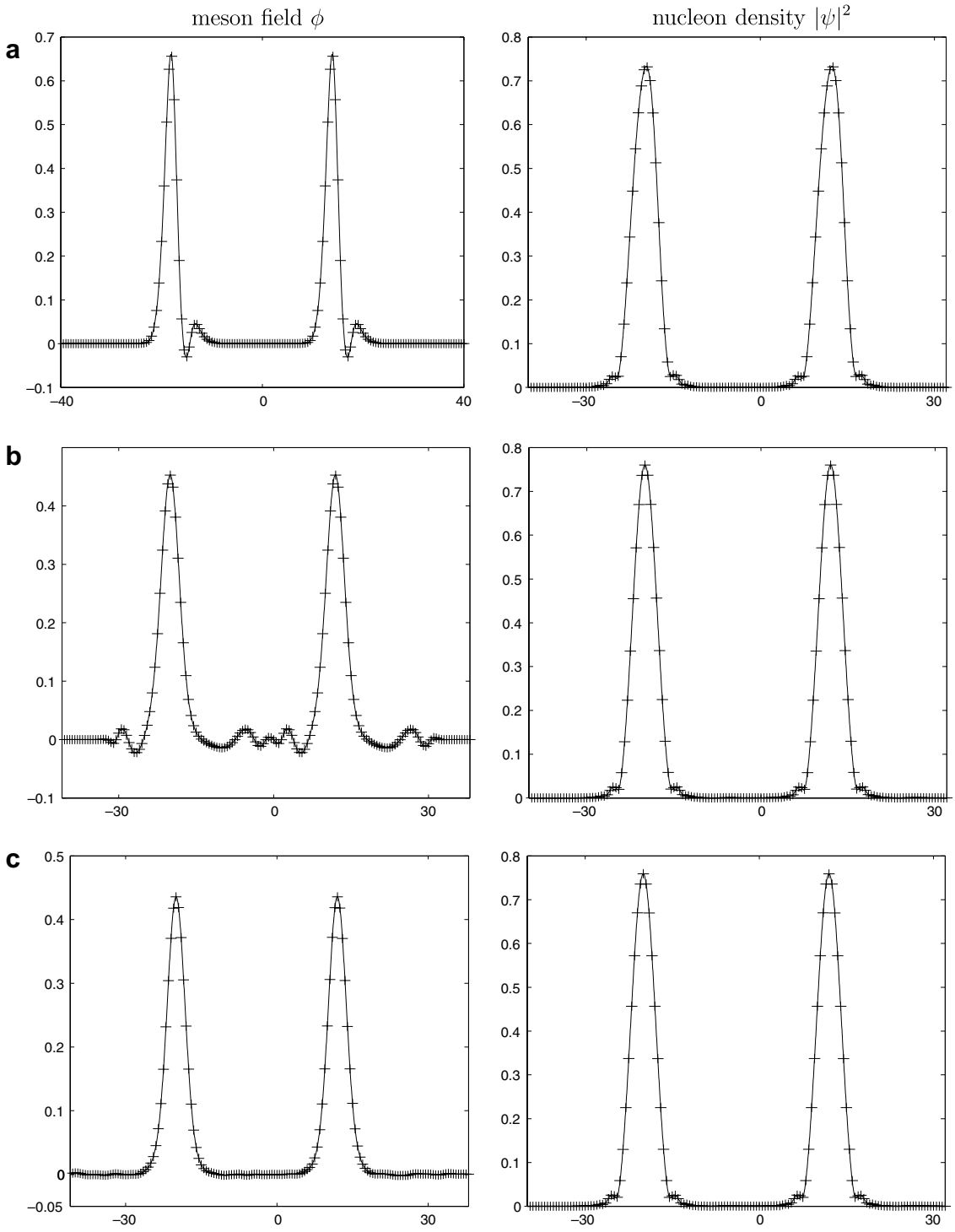

Fig. 2. Numerical solutions at $t = 1$ for Example 1 with Type 2 initial data in the 'nonrelativistic' limit regime by PSAS–TSSP with the meshing strategy $h = 1/2$ and $k = 0.005$ which are both independent of ε. '−': exact solution, '+++': numerical solution. (a): $\varepsilon = 1/2$; (b): $\varepsilon = 1/16$; and (c) $\varepsilon = 1/128$.

(ii) In the 'nonrelativistic' limit regime, i.e. $0 < \varepsilon \ll 1$, the ε-resolution of our numerical methods PSAS–TSSP and CN–LF–TSSP with $\beta = 1/4$ or $1/2$ is $h = O(\varepsilon)$ and $k = O(\varepsilon)$ for initial data with $O(\varepsilon)$-wavelength, and resp., $h = O(1)$ and $k = O(1)$ for well-prepared initial data with $O(1)$-wavelength. The method CN–LF–TSSP with $\beta = 0$ gives correct numerical results only at meshing strategy $h = O(\varepsilon)$ and $k = O(\varepsilon^2)$ for initial data with $O(\varepsilon)$-wavelength, and resp., $h = O(1)$ and $k = O(\varepsilon)$ for well-prepared initial data with $O(1)$-wavelength.

Thus, in the following subsections, we always use PSAS–TSSP for solving KGS.

5.2. Convergence in 'nonrelativistic' limit regime ($0 < \varepsilon \ll 1$)

Example 2. Reduction from KGS equations to S–Y equations and quadratic convergence rate in the nonrelativistic limit regime, i.e., we choose $d = 1$, $v = 0$ and $\gamma = 0$ in (1.1) and (1.2). We solve the KGS (1.1) and (1.2) in 1D with the initial condition in (1.3) chosen as (5.2) and (5.3) and the S–Y (2.13) and (2.14) in 1D with the initial condition chosen as (5.2) in the interval $[-80, 80]$ with mesh size $h = 5/128$ and time step $k = 0.0005$. We take $p = 8$ in (5.2). Here the initial data for KGS is compatible with those for its limiting S–Y equations, i.e. well-prepared initial data. Let ψ^{KGS} and ϕ^{KGS} be the numerical solutions of the KGS (1.1) and (1.2), and ψ^{SY} and ϕ^{SY} of the S–Y (2.13) and (2.14) by using PSAS–TSSP and TSSP [1,5], respectively. Table 4 shows the errors between the solutions of the KGS and its reduction S–Y at time $t = 1.0$ under different ε.

From Table 4, we can see that the nucleon field ψ^{KGS}, meson field ϕ^{KGS} and the Hamiltonian H^{KGS} of KGS (1.1) and (1.2) converge to ψ^{SY} in l^2-norm, ϕ^{SY} in l^2-norm and H^{SY} of the S–Y (2.13) and (2.14) quadratically in the 'nonrelativistic' limit regime, i.e., $0 < \varepsilon \ll 1$, respectively, provided that the initial data in (1.3) satisfy (5.4) and $\psi^{(0)}$ is with $O(1)$-wavelength, i.e. well-prepared initial data. These confirm the formal analysis in (2.14) and (2.17). In contrast, from our additional numerical results not shown here, when $\varepsilon = O(1)$ or $\varepsilon = O(1)$ with ill-prepared initial data (e.g. (5.4) is not satisfied or $\psi^{(0)}$ is with $O(\varepsilon)$-wavelength), the solutions of the KGS are far away from the solution of the S–Y equations (cf. Fig. 7).

5.3. Applications

Example 3. The standard KGS with a plane-wave solution, i.e., we choose $d = 1$, $\varepsilon = 1$, $v = 0$ and $\gamma = 0$ in (1.1)–(1.3) and consider the problem on the interval $[a, b]$ with $a = 0$ and $b = 2\pi$. The initial condition is taken as

$$\psi(x, 0) = \psi^{(0)}(x) = \mathrm{e}^{i7x}, \quad \phi(x, 0) = \phi^{(0)}(x) = 1, \quad \phi_t(x, 0) = \phi^{(1)}(x) = 0. \tag{5.5}$$

It is easy to see that KGS (3.1), (3.2) with periodic boundary conditions (3.3), (3.4) and initial condition (5.5) admits the plane-wave solution

$$\psi(x, t) = \mathrm{e}^{i(7x - 48t)}, \quad \phi(x, t) = 1, \quad a \leqslant x \leqslant b, \quad t \geqslant 0. \tag{5.6}$$

We solve this problem by using the PSAS–TSSP (3.25), (3.26) with mesh size $h = \frac{\pi}{8}$, time step $k = 0.001$. Fig. 3 shows the numerical results at $t = 2$ and $t = 4$.

From Fig. 3, we can see that the PSAS–TSSP method for KGS really provides the exact plane-wave solution of the KGS (3.1)–(3.5).

Table 4
Error analysis between KGS and its reduction S–Y: errors are computed at time $t = 1.0$ under $h = 5/128$ and $k = 0.0005$

	$\varepsilon_0 = 1/4$	$\varepsilon_0/2$	$\varepsilon_0/4$	$\varepsilon_0/8$
$\|\phi^{\mathrm{KGS}} - \phi^{\mathrm{SY}}\|_{l^2}$	0.357	3.26E − 2	7.762E − 3	1.809E − 4
$\|\psi^{\mathrm{KGS}} - \psi^{\mathrm{SY}}\|_{l^2}$	3.261E − 2	7.597E − 3	1.399E − 3	3.373E − 4
$\|H - H^{\mathrm{SY}}\|$	0.165	3.314E − 2	8.721E − 3	2.492E − 4

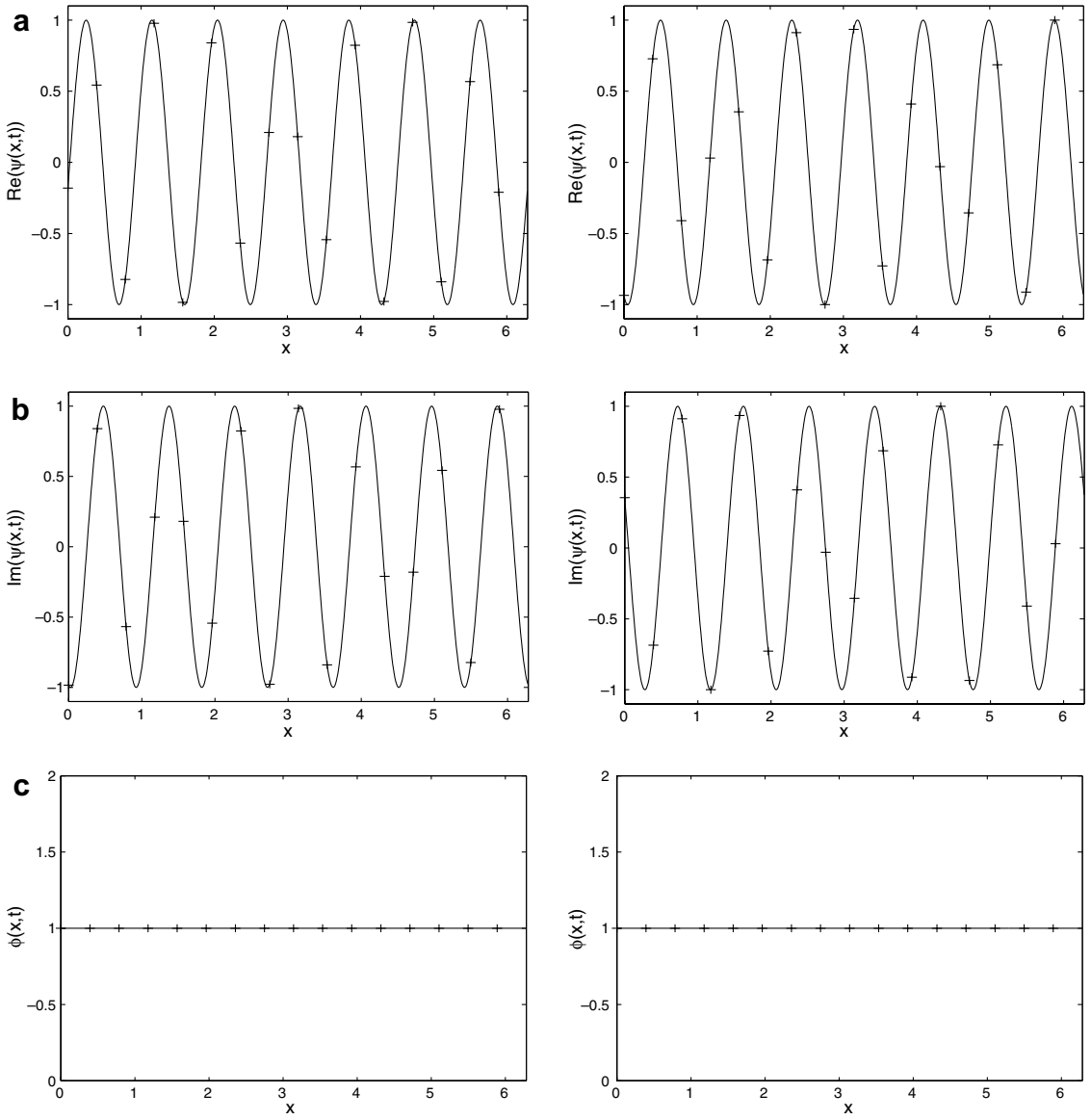

Fig. 3. Numerical solutions for the plane wave of KGS in Example 3 at time $t = 2$ (left column) and $t = 4$ (right column). '–': exact solution given in (5.6), '+++': numerical solution. (a): Real part of nucleon filed $\mathrm{Re}(\psi(x,t))$; (b): imaginary part of nucleon field $\mathrm{Im}(\psi(x,t))$; and (c): meson filed ϕ.

Example 4. Interaction between solitary-wave solutions in 1D for the standard KGS, i.e., we choose $d = 1$, $\varepsilon = 1$, $\nu = 0$ and $\gamma = 0$ in (3.1)–(3.3). The initial condition is chosen as

$$\psi(x,0) = \psi_+(x+p, t=0) + \psi_-(x-p, t=0), \tag{5.7}$$

$$\phi(x,0) = \phi_+(x+p, t=0) + \phi_-(x-p, t=0), \quad x \in \mathbb{R}, \tag{5.8}$$

$$\partial_t\phi(x,0) = \partial_t\phi_+(x+p, t=0) + \partial_t\phi_-(x-p, t=0), \tag{5.9}$$

where $\psi_\pm$ and $\phi_\pm$ are defined as in (2.7) and (2.8), and $x = \pm p$ are initial locations of the two solitons. We solve the problem in the interval $[-40, 40]$, i.e., $a = -40$ and $b = 40$ with mesh size $h = 5/128$ and time step $k = 0.001$ by using our method PSAS–TSSP, and take $p = 8$ and $B = 1$. Fig. 4 shows the values of $|\psi(x,t)|$ and $\phi(x,t)$ at different times.

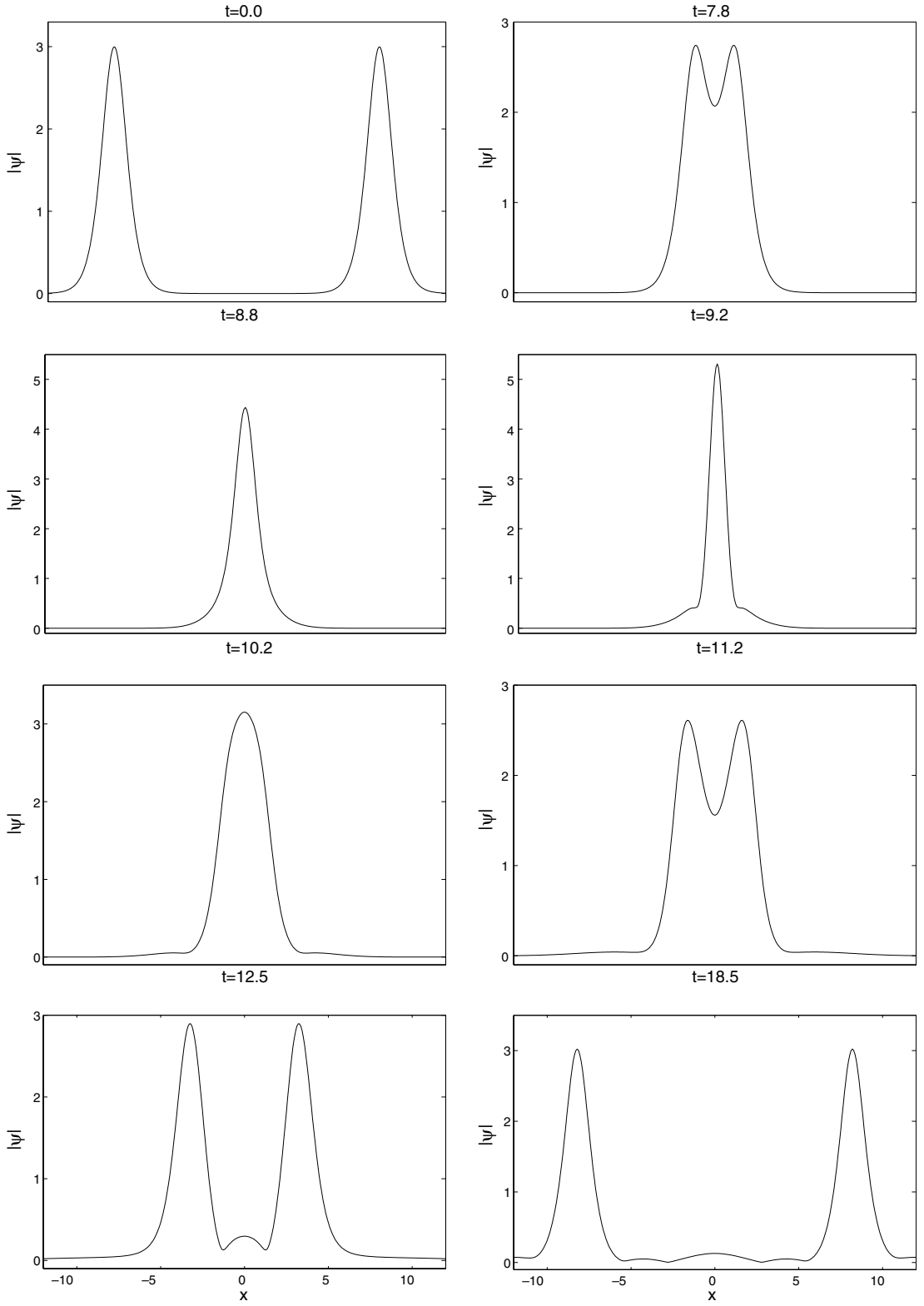

Fig. 4. Numerical solutions of soliton–soliton collision in the standard KGS in Example 4. I: Nucleon density $|\psi(x,t)|$ ('this figure'); II. meson field $\phi(x,t)$ ('continued').

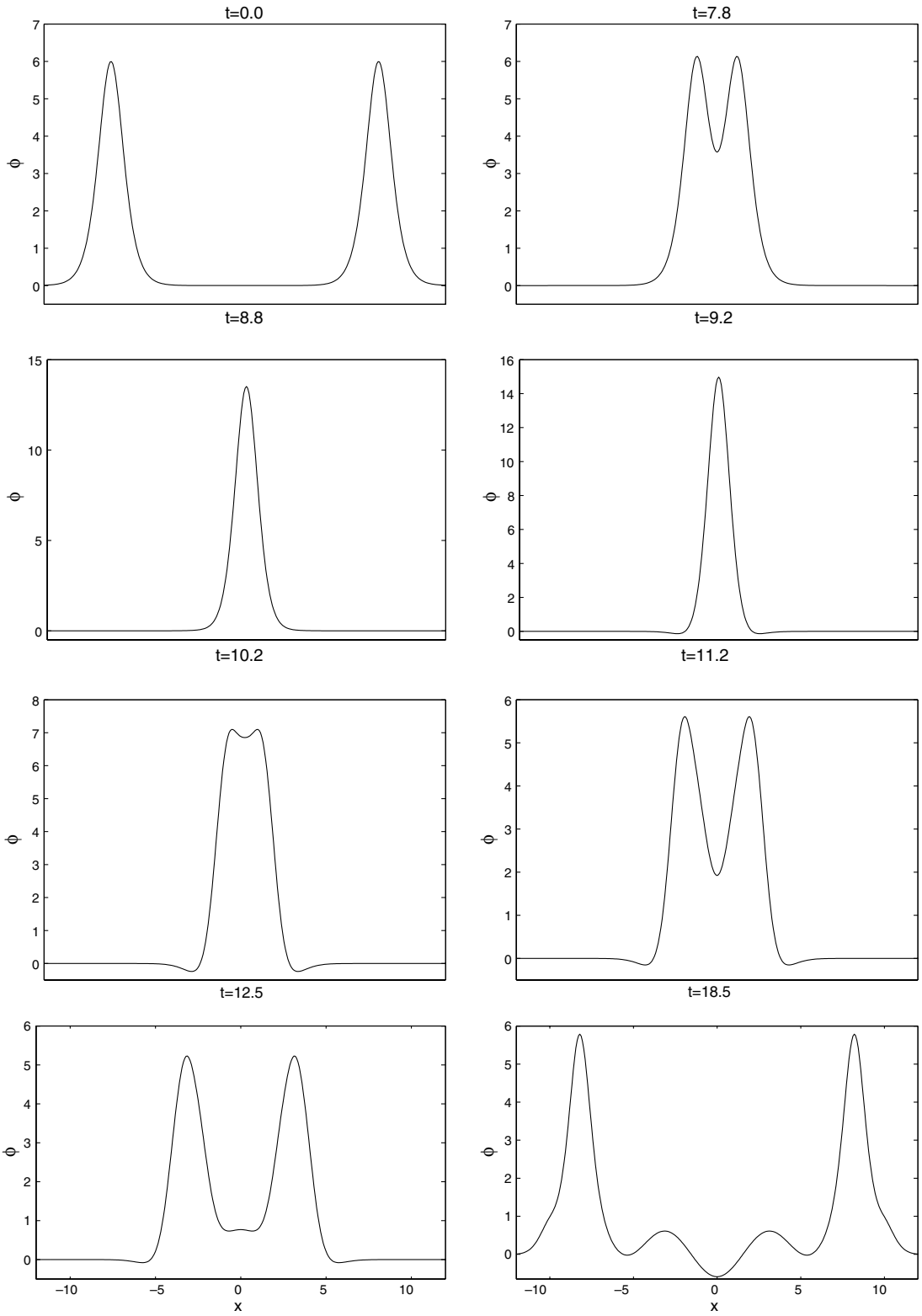

Fig. 4 (*continued*)

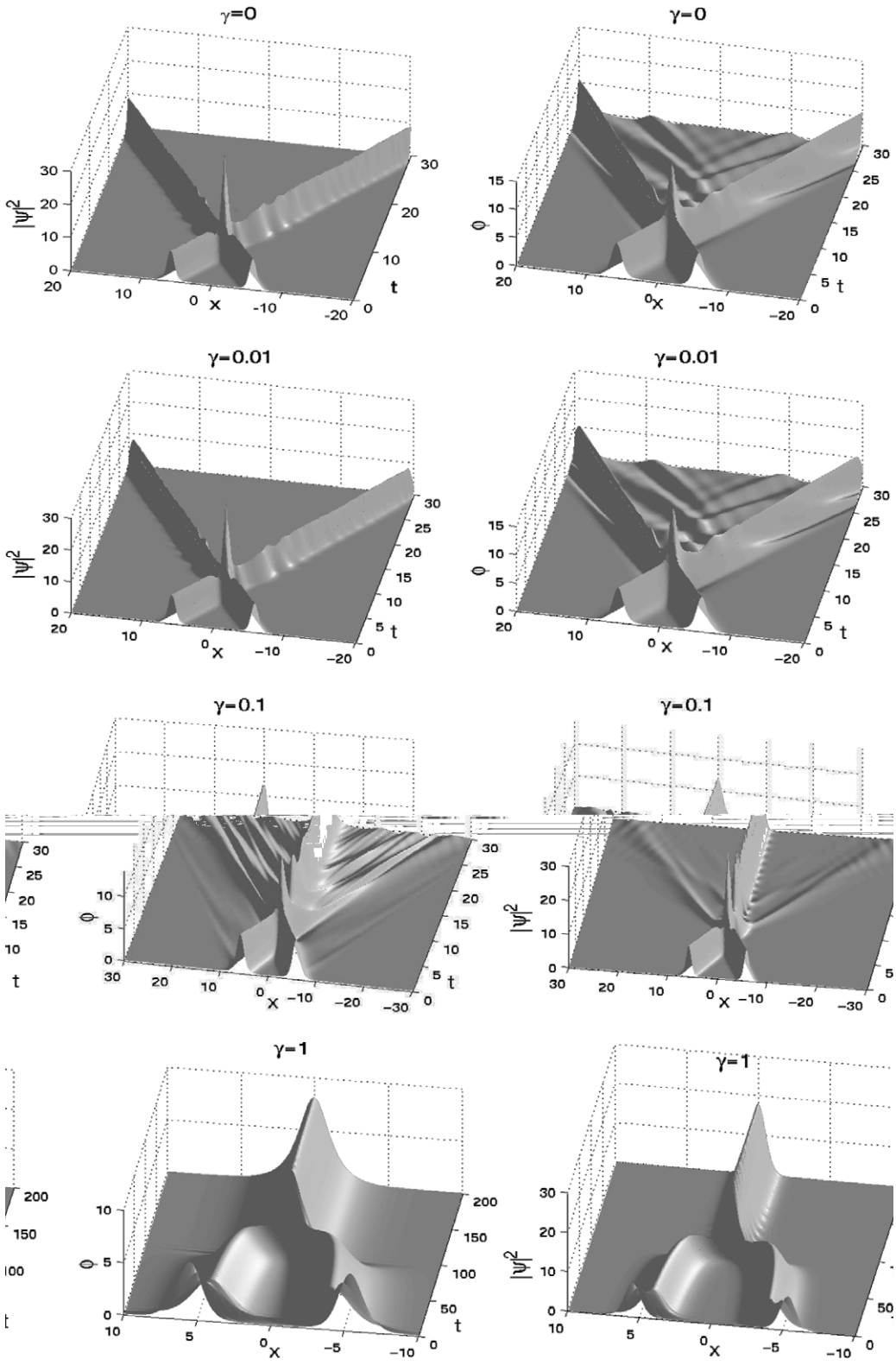

Fig. 5. Time evolution of nucleon density $|\psi(x,t)|^2$ (left column) and meson field $\phi(x,t)$ (right column) for soliton–soliton collision of KGS in Example 4 for different values of γ.

From Fig. 4, the time $t = 9.2$ corresponds to the time when the two solitons are at the same location and the time $t = 18.5$ corresponds to the time when the collision is nearing completion (cf. Fig. 4). From the figure we can see that during the collision, waves are emitted, and that after the collision the two solitons have a reduced peak value.

Example 5. Soliton–soliton collision of KGS with a damping term in 1D, i.e., we choose $d = 1$, $\varepsilon = 1$ and $v = 0$ in (1.1)–(1.3). The initial condition is chosen as (5.7) and (5.8). Again, we solve the problem in the interval $[-40, 40]$, i.e., $a = -40$ and $b = 40$ with mesh size $h = 5/128$ and time step $k = 0.001$ by using our method PSAS–TSSP, and take $p = 8$ and $B = 1$. Fig. 5 displays time evolution of $|\psi(x,t)|^2$ and $\phi(x,t)$ for different values of γ. Fig. 6 shows time evolution of the Hamiltonian $H(t)$ and the mean value of the meson field $N(t)$ for different values of γ.

From Figs. 5 and 6, we can draw the following conclusions: (i) when $\gamma = 0$, the collision between the two solitons seems quite elastic (cf. Fig. 5, top row) although there are some waves are emitted; when $\gamma > 0$ but small, damping effect can be observed in the collision and the emission of sound waves is inconspicuous; when $\gamma > 0$ and large, a soliton wave which is a bound state of the KGS is generated after the collision (cf. Fig. 5 last row). This observation seems new for the KGS. (ii). When $\gamma = 0$, the Hamiltonian is conserved; when $\gamma > 0$, it decreases when time increases and converges to a constant when time goes to infinity (cf. Fig. 6, left). (iii) When $\gamma = 0$, the mean value of the meson field changes periodically; where it oscillates and decays when $\gamma > 0$ (cf. Fig. 6, right). These agree very well with the analytical results in Section 2. (iv) The results here also demonstrate the efficiency and high resolution of our numerical method for studying soliton–soliton collision in KGS.

Example 6. Soliton–soliton collision of KGS in the 'nonrelativistic' limit regime in 1D, i.e., we choose $d = 1$, $\gamma = 0$ and $v = 0$ in (1.1)–(1.3). The initial condition is chosen as

$$\psi(x,0) = \psi^{(0)}(x) = \operatorname{sech}(x+p)e^{-2i(x+p)} + \operatorname{sech}(x-p)e^{-2i(x-p)}, \tag{5.10}$$

$$\phi(x,0) = \phi^{(0)}(x) = -|\operatorname{sech}(x+p)|^2 - |\operatorname{sech}(x-p)|^2, \quad \partial_t\phi(x,0) = 0. \tag{5.11}$$

Notice that the above $\phi^{(0)}$ does not satisfy (5.4), i.e. the initial data here is ill-prepared. We solve the problem in the interval $[-128, 128]$, i.e., $a = -128$ and $b = 128$ with mesh size $h = 1/8$ and time step $k = 0.0005$ by using our method PSAS–TSSP, and take $p = 16$ in (5.10). Fig. 7 displays time evolution of $|\psi(x,t)|^2$ and $\phi(x,t)$ for different values of ε.

From Fig. 7, we can see that waves with $O(\varepsilon)$-wavelength are generated in the meson field although the initial data are with $O(1)$-wavelength without satisfying (5.4). This implies that in this case the KGS can not be reduced to S–Y when $\varepsilon \to 0$.

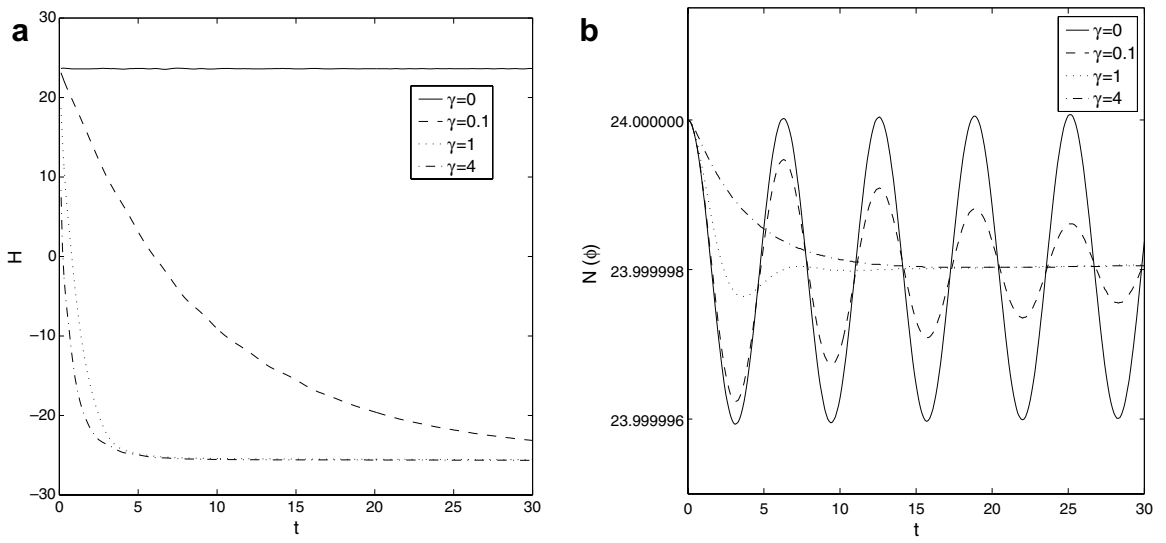

Fig. 6. Time evolution of the Hamiltonian $H(t)$ (left) and the mean value of the meson field $N(t)$ (right) in Example 4 for different values of γ.

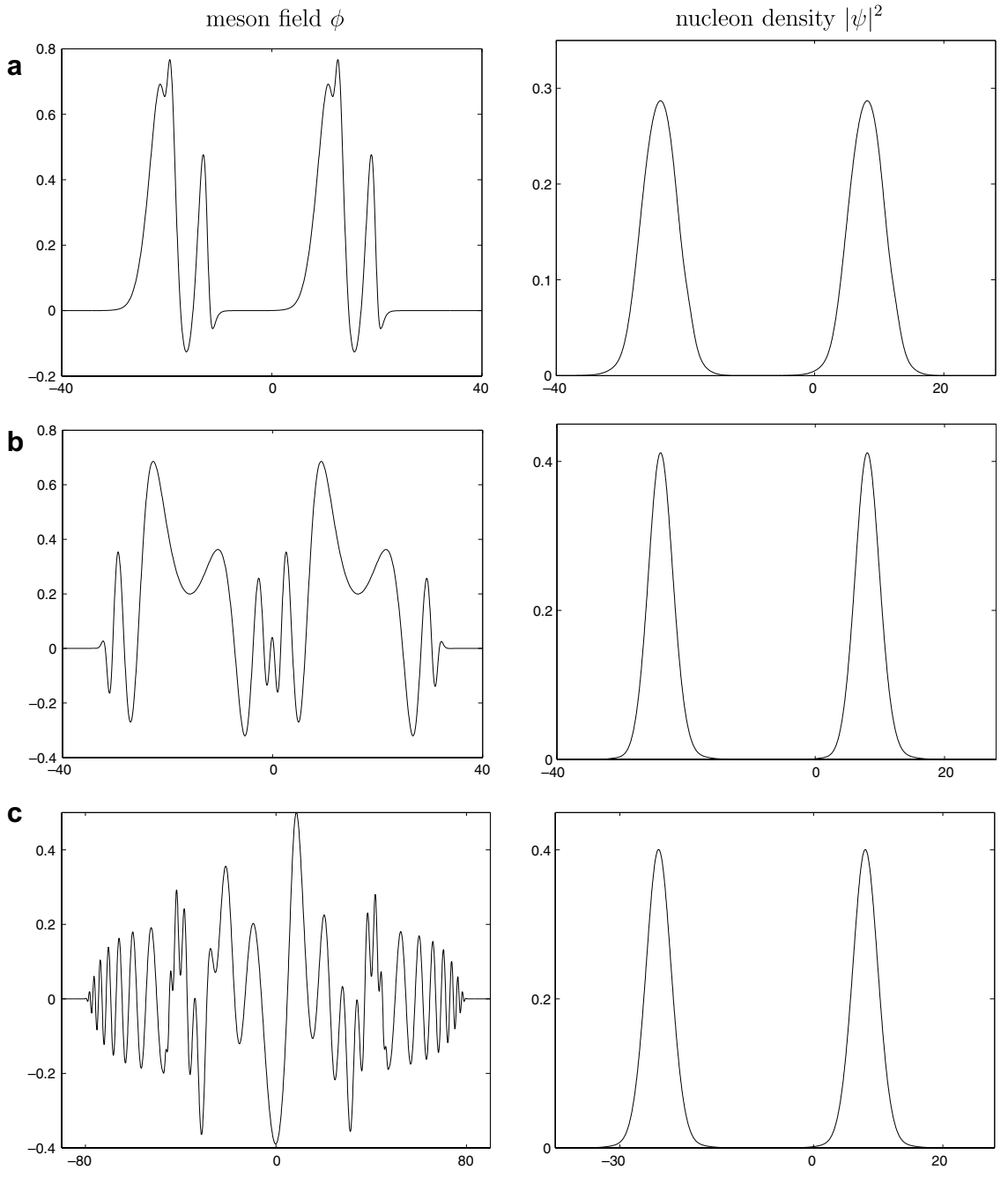

Fig. 7. Numerical solutions at $t = 2$ for Example 6 in the 'nonrelativistic' limit regime by PSAS–TSSP for different ε. (a): $\varepsilon = 1/2$; (b): $\varepsilon = 1/8$; and (c): $\varepsilon = 1/32$.

Example 7. Dynamics of KGS in 2D, i.e., we choose $d = 2$, $v = 0$ and $\varepsilon = 1$ in (1.1)–(1.3). The initial condition is taken as

$$\psi(x,y,0) = \frac{2}{e^{x^2+2y^2} + e^{-(x^2+2y^2)}} e^{i5/\cosh(\sqrt{4x^2+y^2})},$$

$$\phi(x,y,0) = e^{-(x^2+y^2)}, \quad \phi_t(x,y,0) = \frac{e^{-(x^2+y^2)}}{2}, \quad (x,y) \in \mathbb{R}^2.$$

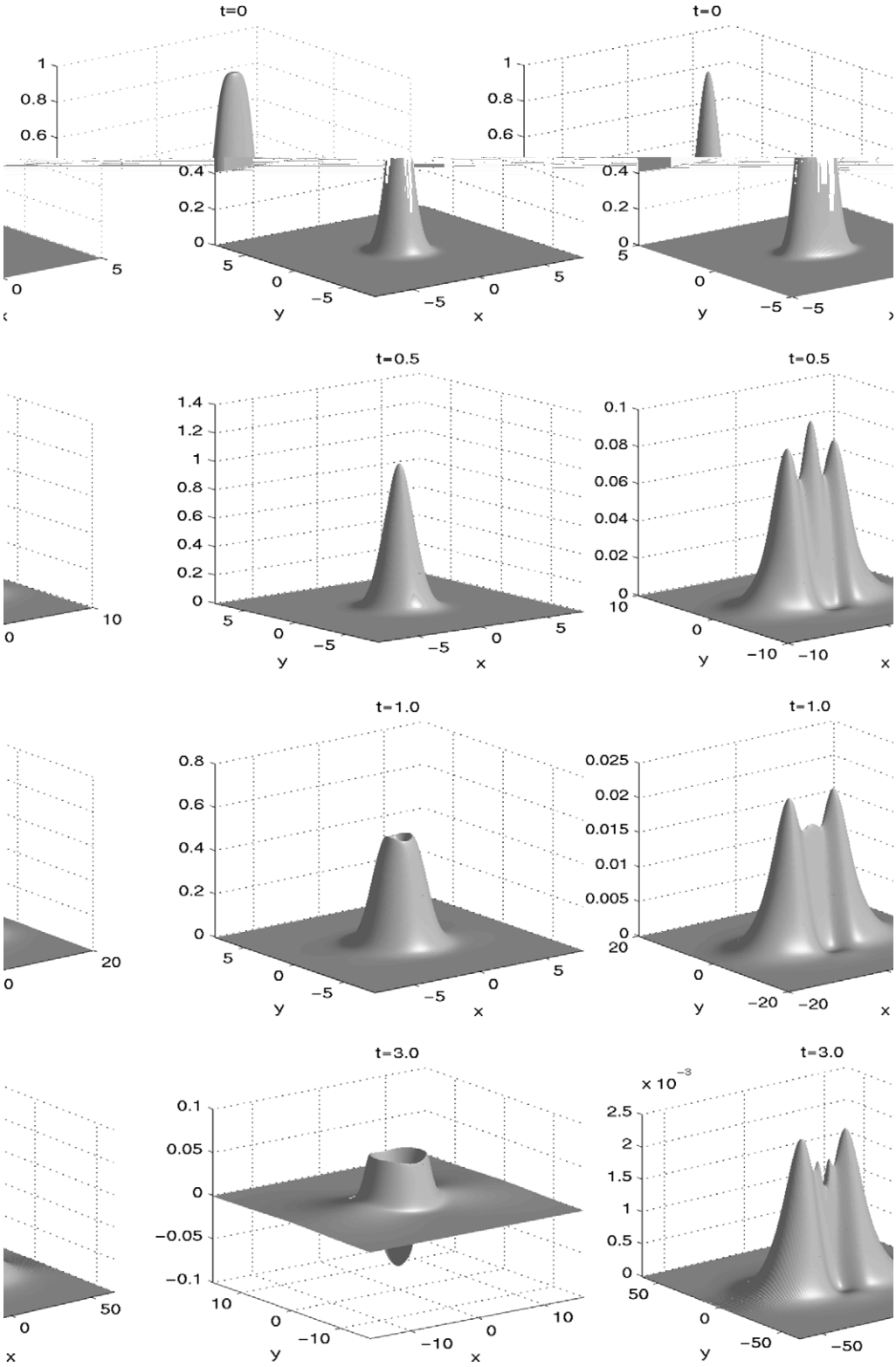

Fig. 8. Surface plots of the nucleon density $|\psi(x,y,t)|^2$ (left column) and meson field $\phi(x,y,t)$ (right column) in Example 5 with $\gamma = 0$ at different times.

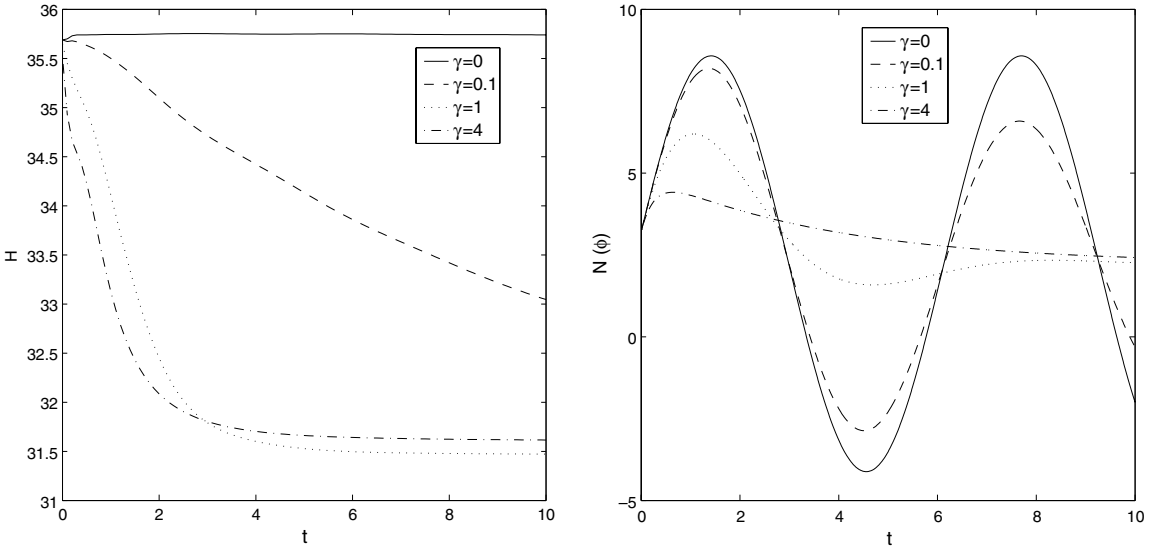

Fig. 9. Time evolution of the Hamiltonian $H(t)$ (left) and the mean value of the meson field $N(t)$ (right) in Example 5 for different values of γ.

We solve this problem on the rectangle $[-64, 64]^2$ with mesh size $h = 1/16$ and time step $k = 0.001$ by using our method PSAS–TSSP. Fig. 8 shows the surface plots of ϕ and $|\psi|^2$ with $\gamma = 0$ at different times. Fig. 9 depicts time evolution of the Hamiltonian $H(t)$ and the mean value of the meson field $N(t)$ for different values of γ.

From Figs. 8 and 9, we can draw the following conclusions: (i) when $\gamma = 0$, the Hamiltonian is conserved; when $\gamma > 0$, it decreases when time increases and converges to a constant when time goes to infinity (cf. Fig. 8, left). (ii) when $\gamma = 0$, the mean value of the meson field changes periodically; where it oscillates and decays when $\gamma > 0$ (cf. Fig. 8, right). These agree very well with the analytical results in Section 2. (iii) The results here also demonstrate the efficiency and high resolution of our numerical method for studying the dynamics of KGS in 2D and 3D.

6. Conclusion

We have studied the dynamics of the Klein–Gordon–Schrödinger (KGS) equations both analytically and numerically. Along the analytical front, we studied the dynamics of the mean value of the meson field. On the numerical side, we proposed two efficient and accurate numerical methods for discretizing the KGS equations. The methods are explicit, unconditionally stable, of spectral accuracy in space and second-order accuracy in time, easy to extend to high dimensions, easy to program, less memory-demanding, and time reversible and time transverse invariant. Furthermore, they conserve (or keep the same decay rate of) the wave energy in KGS when there is no damping (or a linear damping) term, give exact results for the plane-wave solution of KGS, and keep the same dynamics of the mean value of the meson field in the discretized level. We also applied our new numerical methods to study numerically soliton-soliton interaction of KGS in 1D and the dynamics of KGS in 2D. We numerically found that, when a large damping term is added to the Klein–Gordon equation, bound state of KGS can be obtained from the dynamics of KGS when time goes to infinity. In the future, these efficient and accurate numerical methods can be used to compute bound state of KGS and to study the dynamics and wave interaction of KGS in 3D.

Acknowledgement

The authors acknowledge support by the National University of Singapore Grant No. R-146-000-083-112.

Appendix A. Proof of Theorem 4.2 in Section 4

Proof. From (4.1), (3.25) and (3.27), noticing the orthogonality of the discrete Fourier series, we have

$$N(\phi^{m+1}) = \frac{b-a}{M}\sum_{j=0}^{M-1}\phi_j^{m+1} = \frac{b-a}{M}\sum_{j=0}^{M-1}\sum_{l=-M/2}^{M/2-1}\widetilde{(\phi^{m+1})}_l\, e^{i\mu_l(x_j-a)} = \frac{b-a}{M}\sum_{l=-M/2}^{M/2-1}\widetilde{(\phi^{m+1})}_l\sum_{j=0}^{M-1}e^{i\mu_l(x_j-a)}$$
$$= (b-a)\widetilde{(\phi^{m+1})}_0. \tag{A.1}$$

Similarly, from (4.2) with $v=0$, we have

$$\widetilde{\left(|\psi^{m+1}|^2\right)}_0 = \frac{1}{M}\sum_{j=0}^{M-1}|\psi_j^{m+1}|^2 = \frac{\|\psi^{m+1}\|_{l^2}^2}{b-a} = \frac{\|\psi^0\|_{l^2}^2}{b-a} = \widetilde{\left(|\psi^{(0)}|^2\right)}_0, \quad m\geqslant 0. \tag{A.2}$$

(i) When $\gamma>2$, denote $p=e^{\lambda_1^0 k}$ and $q=e^{\lambda_2^0 k}$. From (3.28) and (3.16) with $l=0$, (2.12) and (A.2), we obtain

$$\widetilde{(\phi^{m+1})}_0 = -pq\widetilde{(\phi^{m-1})}_0 + (p+q)\widetilde{(\phi^m)}_0 + (p-1)(q-1)\widetilde{\left(|\psi^m|^2\right)}_0$$
$$= -pq\widetilde{(\phi^{m-1})}_0 + (p+q)\widetilde{(\phi^m)}_0 + (p-1)(q-1)\widetilde{\left(|\psi^{(0)}|^2\right)}_0, \quad m\geqslant 1; \tag{A.3}$$

$$\widetilde{(\phi^1)}_0 = \frac{p-q}{\lambda_1^0-\lambda_2^0}\widetilde{(\phi^{(1)})}_0 + \frac{\lambda_1^0 q-\lambda_2^0 p}{\lambda_1^0-\lambda_2^0}\widetilde{(\phi^{(0)})}_0 + \left(1+\frac{\lambda_2^0 p-\lambda_1^0 q}{\lambda_1^0-\lambda_2^0}\right)\widetilde{\left(|\psi^{(0)}|^2\right)}_0. \tag{A.4}$$

Rewrite (A.3), by induction, we obtain for $m\geqslant 1$:

$$\widetilde{(\phi^{m+1})}_0 - p\widetilde{(\phi^m)}_0 + (p-1)\widetilde{\left(|\psi^{(0)}|^2\right)}_0 = q\left(\widetilde{(\phi^m)}_0 - p\widetilde{(\phi^{m-1})}_0 + (p-1)\widetilde{\left(|\psi^{(0)}|^2\right)}_0\right)$$
$$= q^m\left(\widetilde{(\phi^1)}_0 - p\widetilde{(\phi^{(0)})}_0 + (p-1)\widetilde{\left(|\psi^{(0)}|^2\right)}_0\right). \tag{A.5}$$

From (A.5), by induction again, we get

$$\widetilde{(\phi^{m+1})}_0 = \sum_{r=0}^{m}\left[p^r q^{m-r}\left(\widetilde{(\phi^1)}_0 - p\widetilde{(\phi^{(0)})}_0\right) + p^r(q^{m-r}-1)(p-1)\widetilde{\left(|\psi^{(0)}|^2\right)}_0\right] + p^{m+1}\widetilde{(\phi^{(0)})}_0$$
$$= \frac{q^{m+1}-p^{m+1}}{q-p}\widetilde{(\phi^1)}_0 + \frac{qp^{m+1}-pq^{m+1}}{q-p}\widetilde{(\phi^{(0)})}_0 + \frac{p^{m+1}-q^{m+1}+pq^{m+1}-qp^{m+1}+q-p}{q-p}\widetilde{\left(|\psi^{(0)}|^2\right)}_0. \tag{A.6}$$

Combining (A.1), (A.6) and (A.4), noticing (A.2) and (4.1), we obtain

$$N(\phi^{m+1}) = \frac{q^{m+1}-p^{m+1}}{q-p}\left[\frac{p-q}{\lambda_1^0-\lambda_2^0}N(\phi^{(1)}) + \frac{\lambda_1^0 q-\lambda_2^0 p}{\lambda_1^0-\lambda_2^0}N(\phi^{(0)}) + \left(1+\frac{\lambda_2^0 p-\lambda_1^0 q}{\lambda_1^0-\lambda_2^0}\right)N(|\psi^{(0)}|^2)\right]$$
$$+\frac{qp^{m+1}-pq^{m+1}}{q-p}N(\phi^{(0)}) + \frac{p^{m+1}-q^{m+1}+pq^{m+1}-qp^{m+1}+q-p}{q-p}N(|\psi^{(0)}|^2)$$

$$= \frac{p^{m+1}-q^{m+1}}{\lambda_1^0-\lambda_2^0}N(\phi^{(1)}) + \frac{\lambda_1^0 q^{m+1}-\lambda_2^0 p^{m+1}}{\lambda_1^0-\lambda_2^0}N(\phi^{(0)}) + \left(1-\frac{\lambda_1^0 q^{m+1}-\lambda_2^0 p^{m+1}}{\lambda_1^0-\lambda_2^0}\right)N(|\psi^{(0)}|^2)$$

$$= N(|\psi^{(0)}|^2) + \frac{-N(\phi^{(1)})+\lambda_1^0(N(\phi^{(0)})-N(|\psi^{(0)}|^2))}{\lambda_1^0-\lambda_2^0}e^{\lambda_2^0 t_{m+1}} + \frac{N(\phi^{(1)})-\lambda_2^0(N(\phi^{(0)})-N(|\psi^{(0)}|^2))}{\lambda_1^0-\lambda_2^0}e^{\lambda_1^0 t_{m+1}}. \quad (A.7)$$

Thus, (4.3) is a combination of (A.7) and (4.6).

(ii) When $\gamma = 2$, denote $p = e^{\lambda_0 k}$. From (3.29) and (3.16) with $l = 0$, (2.12) and (A.2), we obtain

$$\widetilde{(\phi^{m+1})}_0 = -p^2\widetilde{(\phi^{m-1})}_0 + 2p\widetilde{(\phi^m)}_0 + (p-1)^2\widetilde{\left(|\psi^m|^2\right)}_0$$

$$= -p^2\widetilde{(\phi^{m-1})}_0 + 2p\widetilde{(\phi^m)}_0 + (p-1)^2\widetilde{\left(|\psi^{(0)}|^2\right)}_0, \quad m \geqslant 1; \quad (A.8)$$

$$\widetilde{(\phi^1)}_0 = kp\widetilde{\left(\phi^{(1)}\right)}_0 + (1-\lambda_0 k)p\widetilde{\left(\phi^{(0)}\right)}_0 + (1-(1-\lambda_0 k)p)\widetilde{\left(|\psi^{(0)}|^2\right)}_0. \quad (A.9)$$

Rewrite (A.8), by induction, we obtain for $m \geqslant 1$:

$$\widetilde{(\phi^{m+1})}_0 - p\widetilde{(\phi^m)}_0 + (p-1)\widetilde{\left(|\psi^{(0)}|^2\right)}_0 = p\left(\widetilde{(\phi^m)}_0 - p\widetilde{(\phi^{m-1})}_0 + (p-1)\widetilde{\left(|\psi^{(0)}|^2\right)}_0\right)$$

$$= p^m\left(\widetilde{(\phi^1)}_0 - p\widetilde{\left(\phi^{(0)}\right)}_0 + (p-1)\widetilde{\left(|\psi^{(0)}|^2\right)}_0\right). \quad (A.10)$$

From (A.10), by induction again, we get

$$\widetilde{(\phi^{m+1})}_0 = \sum_{r=0}^{m}\left[p^m\left(\widetilde{(\phi^1)}_0 - p\widetilde{\left(\phi^{(0)}\right)}_0\right) + p^r(p^{m-r}-1)(p-1)\widetilde{\left(|\psi^{(0)}|^2\right)}_0\right] + p^{m+1}\widetilde{\left(\phi^{(0)}\right)}_0$$

$$= (m+1)p^m\widetilde{(\phi^1)}_0 - mp^{m+1}\widetilde{\left(\phi^{(0)}\right)}_0 + (1-p^{m+1}+(m+1)(p-1)p^m)\widetilde{\left(|\psi^{(0)}|^2\right)}_0. \quad (A.11)$$

Combining (A.1), (A.11) and (A.9), noticing (A.2) and (4.1), we obtain

$$N(\phi^{m+1}) = (m+1)p^m[kpN(\phi^{(1)}) + (1-\lambda_0 k)pN(\phi^{(0)}) + (1-(1-\lambda_0 k)p)N(|\psi^{(0)}|^2)] - mp^{m+1}N(\phi^{(0)})$$
$$+ [1-p^{m+1}+(m+1)(p-1)p^m]N(|\psi^{(0)}|^2)$$
$$= (m+1)kp^{m+1}N(\phi^{(1)}) \quad + (1-(m+1)\lambda_0 k)p^{m+1}N(\phi^{(0)}) + [1-p^{m+1}+(m+1)\lambda_0 kp^{m+1}]N(|\psi^{(0)}|^2)$$
$$= N(|\psi^{(0)}|^2) + [N(\phi^{(0)}) - N(|\psi^{(0)}|^2)]e^{\lambda_0 t_{m+1}} + [N(\phi^{(1)}) - \lambda_0(N(\phi^{(0)}) - N(|\psi^{(0)}|^2))]t_{m+1}e^{\lambda_0 t_{m+1}}. \quad (A.12)$$

Thus, (4.4) is a combination of (A.12) and (4.6).

(iii) When $0 \leq \gamma < 2$, denote $p = e^{(\lambda_0+i\beta_0)k}$ and $q = e^{(\lambda_0-i\beta_0)k}$. From (3.30) and (3.16) with $l = 0$, (2.12) and (A.2), we obtain

$$\widetilde{(\phi^{m+1})}_0 = -pq\widetilde{(\phi^{m-1})}_0 + (p+q)\widetilde{(\phi^m)}_0 + (p-1)(q-1)\widetilde{\left(|\psi^m|^2\right)}_0$$

$$= -pq\widetilde{(\phi^{m-1})}_0 + (p+q)\widetilde{(\phi^m)}_0 + (p-1)(q-1)\widetilde{\left(|\psi^{(0)}|^2\right)}_0, m \geqslant 1; \quad (A.13)$$

$$\widetilde{(\phi^1)}_0 = \frac{\sin(\beta_0 k)e^{\lambda_0 k}}{\beta_0}\widetilde{\left(\phi^{(1)}\right)}_0 + \left(\cos(\beta_0 k) - \frac{\lambda_0}{\beta_0}\sin(\beta_0 k)\right)e^{\lambda_0 k}\widetilde{\left(\phi^{(0)}\right)}_0$$
$$+ \left[1-\left(\cos(\beta_0 k) - \frac{\lambda_0}{\beta_0}\sin(\beta_0 k)\right)e^{\lambda_0 k}\right]\widetilde{\left(|\psi^{(0)}|^2\right)}_0. \quad (A.14)$$

Rewrite (A.13), by induction, we obtain for $m \geqslant 1$:

$$\begin{aligned}\widetilde{(\phi^{m+1})}_0 - p\widetilde{(\phi^m)}_0 + (p-1)\widetilde{\left(|\psi^{(0)}|^2\right)}_0 &= q(\widetilde{(\phi^m)}_0 - p\widetilde{(\phi^{m-1})}_0 + (p-1)\widetilde{\left(|\psi^{(0)}|^2\right)}_0) \\ &= q^m(\widetilde{(\phi^1)}_0 - p\widetilde{\left(\phi^{(0)}\right)}_0 + (p-1)\widetilde{\left(|\psi^{(0)}|^2\right)}_0). \end{aligned} \tag{A.15}$$

From (A.15), by induction again, we get

$$\begin{aligned}\widetilde{(\phi^{m+1})}_0 &= \sum_{r=0}^{m}\left[p^r q^{m-r}\left(\widetilde{(\phi^1)}_0 - p\widetilde{\left(\phi^{(0)}\right)}_0\right) + p^r(q^{m-r}-1)(p-1)\widetilde{\left(|\psi^{(0)}|^2\right)}_0\right] + p^{m+1}\widetilde{\left(\phi^{(0)}\right)}_0 \\ &= \frac{q^{m+1}-p^{m+1}}{q-p}\widetilde{(\phi^1)}_0 + \frac{qp^{m+1}-pq^{m+1}}{q-p}\widetilde{\left(\phi^{(0)}\right)}_0 + \frac{p^{m+1}-q^{m+1}+pq^{m+1}-qp^{m+1}+q-p}{q-p}\widetilde{\left(|\psi^{(0)}|^2\right)}_0. \end{aligned} \tag{A.16}$$

Combining (A.1), (A.16) and (A.14), noticing (A.2) and (4.1), we obtain

$$\begin{aligned}N(\phi^{m+1}) &= \frac{q^{m+1}-p^{m+1}}{q-p}\left[\left(1-\left(\cos(\beta_0 k)-\frac{\lambda_0}{\beta_0}\sin(\beta_0 k)\right)e^{\lambda_0 k}\right)N(|\psi^{(0)}|^2) + \frac{\sin(\beta_0 k)e^{\lambda_0 k}}{\beta_0}N(\phi^{(1)})\right. \\ &\quad \left.+\left(\cos(\beta_0 k)-\frac{\lambda_0}{\beta_0}\sin(\beta_0 k)\right)e^{\lambda_0 k}N(\phi^{(0)})\right] + \frac{p^{m+1}-q^{m+1}+pq^{m+1}-qp^{m+1}+q-p}{q-p}N(|\psi^{(0)}|^2) \\ &\quad + \frac{qp^{m+1}-pq^{m+1}}{q-p}N(\phi^{(0)}) = e^{\lambda_0(m+1)k}\left(\cos((m+1)\beta_0 k)-\frac{\lambda_0}{\beta_0}\sin((m+1)\beta_0 k)\right)N(\phi^{(0)}) \\ &\quad + \left[1-e^{\lambda_0(m+1)k}\left(\cos((m+1)\beta_0 k)-\frac{\lambda_0}{\beta_0}\sin((m+1)\beta_0 k)\right)\right]N(|\psi^{(0)}|^2) \\ &\quad + e^{\lambda_0(m+1)k}\left(\frac{\sin((m+1)\beta_0 k)}{\beta_0}\right)N(\phi^{(1)}) = N(|\psi^{(0)}|^2) + e^{\lambda_0 t_{m+1}}\left[(N(\phi^{(0)})-N(|\psi^{(0)}|^2))\cos(\beta_0 t_{m+1})\right. \\ &\quad \left.+\frac{N(\phi^{(1)})-\lambda_0(N(\phi^{(0)})-N(|\psi^{(0)}|^2))}{\beta_0}\sin(\beta_0 t_{m+1})\right]. \end{aligned} \tag{A.17}$$

Thus, (4.5) is a combination of (A.17) and (4.6). □

Appendix B. Proof of Theorem 4.3 in Section 4

Proof. For the discretization PSAS–TSSP (3.25), (3.26), setting $\widetilde{\left(|\psi^m|^2\right)}_l = 0$ and plugging $\tilde{\phi}_l^{m+1} = \mu\tilde{\phi}_l^m = \mu^2\tilde{\phi}_l^{m-1}$ into (3.28), (3.29) and (3.30) with $|\mu|$ the amplification factor, we obtain:

(i) When $\gamma^2 - 4(\mu_l^2+1) > 0$, the characteristic equation for μ is

$$\mu^2 - (e^{\lambda_1 k} + e^{\lambda_2 k})\mu + e^{(\lambda_1+\lambda_2)k} = 0. \tag{B.1}$$

Solving the above equation, we have

$$\mu_1 = e^{\lambda_1 k}, \quad \mu_2 = e^{\lambda_2 k}. \tag{B.2}$$

Thus, the amplification factor satisfies

$$G_l = \max\{|\mu_1|, |\mu_2|\} = e^{\frac{-\gamma+\sqrt{\gamma^2-4(\mu_l^2+1)}}{2}} \leqslant 1, \quad l = -\frac{M}{2}, \ldots, \frac{M}{2}-1. \tag{B.3}$$

(ii) When $\gamma^2 - 4(\mu_l^2+1) = 0$, the characteristic equation for μ is

$$\mu^2 - 2e^{-\frac{\gamma k}{2}}\mu + e^{-\gamma k} = 0. \tag{B.4}$$

Solving the above equation, we have

$$\mu = e^{-\frac{\gamma k}{2}}.$$

Thus, the amplification factor satisfies

$$G_l = |\mu| = \mathrm{e}^{-\frac{\gamma k}{2}} \leqslant 1, \quad l = -\frac{M}{2}, \ldots, \frac{M}{2} - 1. \tag{B.5}$$

(iii) When $\gamma^2 - 4(\mu_l^2 + 1) < 0$, the characteristic equation for μ is

$$\mu^2 - 2\cos(\beta k)\mathrm{e}^{-\frac{\gamma k}{2}}\mu + \mathrm{e}^{-\gamma k} = 0. \tag{B.6}$$

Solving the above equation, we have

$$\mu = \mathrm{e}^{-\frac{\gamma k}{2}}[\cos(\beta k) \pm \mathrm{i}\sin(\beta k)]. \tag{B.7}$$

Thus, the amplification factor satisfies

$$G_l = |\mu| = \mathrm{e}^{-\frac{\gamma k}{2}}\sqrt{\cos^2(\beta k) + \sin^2(\beta k)} = \mathrm{e}^{-\frac{\gamma k}{2}} \leqslant 1, \quad l = -\frac{M}{2}, \ldots, \frac{M}{2} - 1. \tag{B.8}$$

(B.3), (B.5) and (B.8), together with (4.2), imply that PSAS–TSSP is unconditionally stable for any time step $k > 0$, mesh size $h > 0$ and parameter values $\gamma \geqslant 0$.

Similarly for the discretization CN–LF–TSSP (3.37), (3.38), noting (3.36), we have the characteristic equation

$$\mu^2 - 2\left(1 - \frac{(\mu_l^2 + 1)k^2 + \varepsilon\gamma k}{2k^2\beta(\mu_l^2 + 1) + \varepsilon\gamma k + 2\varepsilon^2}\right)\mu + 1 - \frac{2\varepsilon\gamma k}{2k^2\beta(\mu_l^2 + 1) + \varepsilon\gamma k + 2\varepsilon^2} = 0. \tag{B.9}$$

Solving the above equation, we obtain

$$\mu = 1 - \frac{(\mu_l^2 + 1)k^2 + \varepsilon\gamma k}{2k^2\beta(\mu_l^2 + 1) + \varepsilon\gamma k + 2\varepsilon^2} \pm \sqrt{\left(1 - \frac{(\mu_l^2 + 1)k^2 + \varepsilon\gamma k}{2k^2\beta(\mu_l^2 + 1) + \varepsilon\gamma k + 2\varepsilon^2}\right)^2 - 1 + \frac{2\varepsilon\gamma k}{2k^2\beta(\mu_l^2 + 1) + \varepsilon\gamma k + 2\varepsilon^2}}.$$

When $1/4 \leqslant \beta \leqslant 1/2$ and $\gamma = 0$, we have

$$\left|1 - \frac{(\mu_l^2 + 1)k^2}{2k^2\beta(\mu_l^2 + 1) + 2\varepsilon^2}\right| \leqslant 1, \quad k > 0.$$

Thus,

$$\mu = 1 - \frac{(\mu_l^2 + 1)k^2}{2k^2\beta(\mu_l^2 + 1) + 2\varepsilon^2} \pm \mathrm{i}\sqrt{1 - \left(1 - \frac{(\mu_l^2 + 1)k^2}{2k^2\beta(\mu_l^2 + 1) + 2\varepsilon^2}\right)^2}.$$

This implies that the amplification factor satisfies

$$G_l = |\mu| = \sqrt{\left(1 - \frac{(\mu_l^2 + 1)k^2}{2k^2\beta(\mu_l^2 + 1) + 2\varepsilon^2}\right)^2 + 1 - \left(1 - \frac{(\mu_l^2 + 1)k^2}{2k^2\beta(\mu_l^2 + 1) + 2\varepsilon^2}\right)^2} = 1, \quad l = -M/2, \ldots, M/2 - 1.$$

This, together with (4.2), implies that CN–LP–TSSP with $1/4 \leqslant \beta \leqslant 1/2$ is unconditionally stable. On the other hand, when $0 \leqslant \beta < 1/4$ and $\gamma = 0$, we need the stability condition

$$\left|1 - \frac{(\mu_l^2 + 1)k^2}{2k^2\beta(\mu_l^2 + 1) + 2\varepsilon^2}\right| \leqslant 1, \quad l = -M/2, \ldots, M/2 - 1.$$

This implies that

$$k \leqslant \min_{-M/2 \leqslant l \leqslant M/2-1} \sqrt{\frac{4\varepsilon^2}{(1 - 4\beta)(1 + \mu_l^2)}} = \frac{2h\varepsilon}{\sqrt{(1 - 4\beta)(\pi^2 + h^2)}}.$$

Thus, we get the stability condition (4.7). □

References

[1] W. Bao, D. Jaksch, An explicit unconditionally stable numerical method for solving damped nonlinear Schrödinger equations with a focusing nonlinearity, SIAM J. Numer. Anal. 41 (2003) 1406–1426.
[2] W. Bao, D. Jaksch, P.A. Markowich, Numerical solution of the Gross–Pitaevsikii equation for Bose–Einstein condensation, J. Comput. Phys. 187 (2003) 318–342.
[3] W. Bao, S. Jin, P.A. Markowich, On time-splitting spectral approximations for the Schrödinger equation in the semiclassical regime, J. Comput. Phys. 175 (2002) 487–524.
[4] W. Bao, X.G. Li, An efficient and stable numerical method for the Maxwell–Dirac system, J. Comput. Phys. 199 (2004) 663–687.
[5] W. Bao, F.F. Sun, Efficient and stable numerical methods for the generalized and vector Zakharov system, SIAM J. Sci. Comput. 26 (2005) 1057–1088.
[6] W. Bao, C. Zheng, A time-splitting spectral method for three-wave interactions in media with competing quadratic and cubic nonlinearities, Commun. Comput. Phys. 2 (2007) 123–140.
[7] P. Bechouche, N.J. Mauser, S. Selberg, Non-relativistic limit of Klein–Gordon–Maxerll, preprint.
[8] P. Bechouche, N.J. Mauser, S. Selberg, Non-relativistic limit of Klein-Gordon-Maxerll to Schrödinger-Poisson, preprint.
[9] P. Biler, Attractors for the system of Schrödinger and Klein–Gordon equations with Yukawa coupling, SIAM J. Math. Anal. 21 (1990) 1190–1212.
[10] D.I. Choi, Numerical Studies of Nonlinear Schrödinger and Klein–Gordon Systems: Techniques and Applications, Ph.D. Thesis, The University of Texas at Austin, 1998.
[11] R.J. Cirincione, P.R. Chernoff, Dirac and Klein–Gordon equations: convergence of solutions in the nonrelativistic limit, Commun. Math. Phys. 79 (1981) 33–46.
[12] A. Darwish, E.G. Fan, A series of new explicit exact solutions for the coupled Klein–Gordon–Schrödinger equations, Chaos Soliton Fract 20 (2004) 609–617.
[13] B. Fornberg, T.A. Driscoll, A fast spectral algorithm for nonlinear wave equations with linear dispersion, J. Comput. Phys. 155 (1999) 456–467.
[14] I. Fukuda, M. Tsutsumi, On the Yukawa-coupled Klein–Gordon–Schrödinger equations in three space dimensions, Prof. Jpn. Acad. 51 (1975) 402–405.
[15] I. Fukuda, M. Tsutsumi, On coupled Klein–Gordon–Schrödinger equations II, J. Math. Anal. Appl. 66 (1978) 358–378.
[16] I. Fukuda, M. Tsutsumi, On coupled Klein–Gordon–Schrödinger equations III, Math. Jpn. 24 (1979) 307–321.
[17] B.L. Guo, Global solution for some problem of a class of equations in interaction of complex Schrödinger field and real Klein–Gordon field, Sci. China Ser. A 25 (1982) 97–107.
[18] B.L. Guo, C.X. Miao, Asymptotic behavior of coupled Klein–Gordon–Schrödinger equations, Sci. China Ser. A 25 (1995) 705–714.
[19] B.L. Guo, Y.S. Li, Attractor for dissipative Klein–Gordon–Schrödinger equations in R^3, J. Differ. Equat. 136 (1997) 356–377.
[21] N. Hayashi, W. von Wahl, On the global strong solutions of coupled Klein–Gordon–Schrödinger equations, J. Math. Soc. Jpn. 39 (1987) 489–497.
[22] F.T. Hioe, Periodic solitary waves for two coupled nonlinear Klein–Gordon and Schrödinger equations, J. Phys. A: Math. Gen. 36 (2003) 7307–7330.
[23] Z. Huang, S. Jin, P.A. Markowich, C. Sparber, C. Zheng, A time-splitting spectral scheme for the Maxwell–Dirac system, J. Comput. Phys. 208 (2005) 761–789.
[24] S. Jin, P.A. Markowich, C. Zheng, Numerical simulation of a generalized Zakharov system, J. Comput. Phys. 201 (2004) 376–395.
[25] L.H. Kong, R.X. Liu, Z.L. Xu, Numerical simulation of interaction between Schrödinger field and Klein–Gordon field by multisymplectic method, Appl. Math. Comp. 181 (2006) 342–350.
[27] Y. Li, B. Guo, Asymptotic smoothing effect of solutions to weakly dissiptive Klein–Gordon–Schrödinger equations, J. Math. Ann. Appl. 282 (2003) 256–265.
[28] X.-Q. Liu, S. Jiang, Exact solutions of multi-component nonlinear Schrödinger and Klein–Gordon equations, Appl. Math. Comp. 160 (2005) 875–880.
[29] X.-S. Liu, Y.-Y. Qi, J.-F. He, P.Z. Ding, Recent progress in sympletic algorithms for use in quantum systems, Commun. Comput. Phys. 2 (2007) 1–53.
[30] K.N. Lu, B.X. Wang, Global attractors for the Klein–Gordon–Schrödinger equation in unbounded domains, J. Differ. Equat. 170 (2001) 281–316.
[31] V.G. Makhankov, Dynamics of classical solitons (in non-integrable systems), Phys. Lett. C 35 (1978) 1–128.
[33] M. Ohta, Stability of stationary states for the coupled Klein–Gordon–Schrödinger equations, Non. Anal. 27 (1996) 455–461.
[34] T. Ozawa, Y. Tsutsumi, Asymptotic behaviour of solutions for the coupled Klein-Gordon-Schrödinger equations, Adv. Stud. Pure Math. 23 (1994) 295–305.
[35] G. Strang, On the construction and comparison of difference schemes, SIAM J. Numer. Anal. 5 (1968) 505–517.
[36] T.R. Taha, M.J. Ablowitz, Analytical and numerical aspects of certain nonlinear evolution equations,III. Numerical, nonlinear Schrödinger equation, J. Comput. Phys. 55 (1984) 203–230.
[37] K. Veselic, On the nonrelativistic limit of the bound states of the Klein–Gordon equation, J. Math. Anal. Appl. 96 (1983) 63–84.
[38] J. Wang, Multisymplectic Fourier pseudospectral method for coupled Klein–Gordon–Schrödinger equations, preprint.

[39] M.L. Wang, Y.B. Zhou, The periodic wave solutions for the Klein–Gordon–Schrödinger equations, Phys. Lett. A 318 (2003) 84–92.
[40] X.M. Xiang, Spectral method for solving the system of equations of Schrödinger–Klein–Gordon field, J. Comput. Appl. Math. 21 (1988) 161–171.
[41] L.M. Zhang, Convergence of a conservative difference scheme for a class of Klein–Gordon–Schrödinger equations in one space dimension, Appl. Math. Comput. 163 (2005) 343–355.